A spatial reconstruction technique applicable to microwave radiometry

Research Report
ISSN 0167-9708
Coden: TEUEDE

Eindhoven
University of Technology
Netherlands

Faculty of Electrical Engineering

A Spatial Reconstruction Technique Applicable to Microwave Radiometry

by
P.J.I. de Maagt
H.G. ter Morsche
J.L.M. van den Broek

EUT Report 92-E-257
ISBN 90-6144-257-5
March 1992

Eindhoven University of Technology Research Reports

EINDHOVEN UNIVERSITY OF TECHNOLOGY

Faculty of Electrical Engineering
Eindhoven The Netherlands

ISSN 0167–9708 Coden:TEUEDE

A SPATIAL RECONSTRUCTION TECHNIQUE APPLICABLE TO MICROWAVE RADIOMETRY

by
P.J.I. de Maagt
H.G. ter Morsche
J.L.M. van den Broek

EUT Report 92–E–257
ISBN 90–6144–257–5

EINDHOVEN
March 1992

CIP–GEGEVENS KONINKLIJKE BIBLIOTHEEK, DEN HAAG

Maagt, P.J.I. de

A spatial reconstruction technique applicable to microwave
radiometry/ by P.J.I. de Maagt, H.G. ter Morsche, J.L.M. van den Broek. –
Eindhoven: Eindhoven University of Technology, Faculty of Electrical Engineering.
– Diagr., fig., tab. – (EUT report, ISSN 0167–9708 ; 92–E–257)
Met lit. opg., reg.
ISBN 90–6144–257–5
NUGI 832
Trefw.: radiometrie.

Abstract

This report presents a spatial image reconstruction technique suited to passive microwave radiometry. The objective is to obtain images with spatial resolution comparable to the scale of atmospheric phenomena. The method has been applied to various (noisy) input signals and results are presented in order to illustrate the performance of the technique. Special attention is given to the effect of statistical and systematic errors, in both the measured antenna noise temperature and the antenna pattern, on the reconstruction.

de Maagt, P.J.I. and H.G. ter Morsche, J.L.M. van den Broek
A SPATIAL RECONSTRUCTION TECHNIQUE APPLICABLE TO MICROWAVE RADIOMETRY.
Faculty of Electrical Engineering, Eindhoven University of Technology, The Netherlands,1992.
EUT Report 92–E–257

Address of the authors:
Telecommunications Division,
Faculty of Electrical Engineering,
Eindhoven University of Technology,
P.O. Box 513
5600 MB EINDHOVEN,
The Netherlands.

Acknowledgement

The authors wish to thank dr.ir. M.H.A.J. Herben and prof.dr.ir. G. Brussaard for their valuable help and discussions.

Table of contents

1 Introduction

Passive remote sensing of the atmosphere is based on the natural electromagnetic noise emission of the atmosphere and therefore capable of providing relevant information about atmospheric processes and parameters (such as liquid water content, water vapour content, the air temperature gradient and so on). The use of passive remote sensing was originally restricted to IR–observations, but in recent years the use of microwave radiometry for this purpose has developed rapidly. This is motivated by the lesser extinction of microwaves in clouds in contrast to IR–observations of the cloudy atmosphere which are only capable of giving information of its upper (or lower) boundaries. Another advantage of microwave radiometry lies in the use of these frequencies for satellite communication. It is possible to obtain a prediction of the behaviour of communication links at those frequencies by using the knowledge that is obtained from sensing the atmosphere. A major disadvantage of microwave radiometry is the substantially lower spatial resolution as compared to that of infrared systems.

A partial enhancement of spatial resolution can be obtained by exploiting the relative motion between the observed scene and the microwave radiometer system. Several techniques have been proposed to this end [1]–[5]. However, some techniques use approximations, the validity of which may be questionable; [1] neglects the radiometer receiver properties, [2] uses some trial–and–error constant which are related to the input, [3] needs an a–priori model of the object to be reconstructed, [4] and [5] need some "proper" truncation of a series (in [4] a series of eigenfunctions and in [5] a Fourier series). The purpose of this report is to show the results of research concerning the practical possibilities of spatial reconstruction where as few approximations as possible are made.

In chapter 2, a model for the relationship between a cloud scene and the radiometer output is given. In chapter 3 the reconstruction technique is discussed. As the objective is to obtain images with spatial resolution comparable to the scale of atmospheric/geophysical phenomena, chapter 3 is followed by a discussion of the scales involved and their implications on the reconstruction. Several examples of the performance are given in chapter 5 and results obtained with a focused and axially defocused antenna pattern are compared and discussed. Finally, the conclusions of this research are given in chapter 6.

2 Relation between observed scene and observation instrument

2.1 Basic problems related to noise temperature measurements

Consider a radiometer system (antenna + receiver) which is monitoring a distributed target to be referred to as a "scene" (see figure 2.1). The influence of the radiometer antenna pattern can be given by the following relation:

$$T_A = \frac{1}{4\pi} \int_{4\pi} T(\theta,\phi)G(\theta,\phi)d\Omega \qquad (2.1)$$

where T_A is the antenna noise temperature, $T(\theta,\phi)$ the brightness temperature of the scene and $G(\theta,\phi)$ the radiometer antenna pattern.

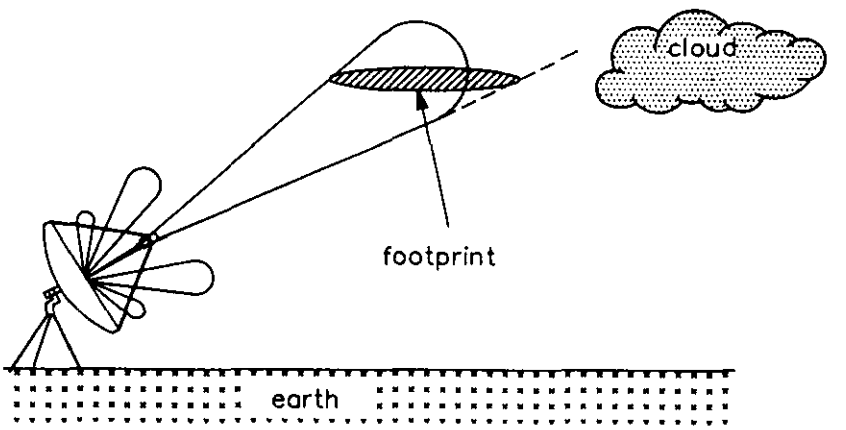

Figure 2.1. Observation of a scene with a radiometer.

Figure 2.1 represents a momentaneous situation, in reality there will be a relative motion between the scene and the radiometer. This enables a sequence of radiometric measurements to be taken for (partially) overlapping positions of the antenna footprints. Where the antenna footprints are taken as the intersection between the scene and the three dimensional antenna pattern at a certain level. As a result the measured antenna temperature is given by the following relation:

$$T_A(t) = \frac{1}{4\pi} \int_{4\pi} T(t,\theta,\phi)G(\theta,\phi)d\Omega \qquad (2.2)$$

Because of the finite dimensions of the antenna, resulting in a non–zero beamwidth, the antenna temperature measured may differ significantly from the brightness temperature of the scene. It is better to say that the measured temperature represents a spatially filtered brightness temperature.
Furthermore, the radiometer receiver integrates the signal T_A in time, and T_A becomes:

$$T_a(t) = \frac{1}{\tau}\int_{t-\frac{\tau}{2}}^{t+\frac{\tau}{2}} T_A(\xi)\, d\xi \qquad (2.3)$$

Where τ is the integration time of the radiometer receiver.

If a more detailed image of the scene is needed, the influences of antenna and receiver have to be cancelled. This leads to inverse methods in microwave imaging. However, the problem inherent to radiometric observation is that the inversion is a very complex matter. To obtain some understanding in this matter it is convenient to enumerate in which way the brightness temperature of the scene is altered before it reaches the output of a radiometer receiver. The different alterations are as follows:

a) addition of cosmic radiation and radiation from the environment, including reflections.
b) alteration of the radiation energy by absorption and attenuation.
c) integration of the scene with the radiation pattern characteristics of the radiometer antenna and receiver.
d) addition of systematic and statistical changes to the detected radiation by the electronic components of the detection equipment.

If a) and b) are taken for granted, the problem can now be stated as eliminating (or at least reducing) the influences c) and d).
To visualize the problem related with c), consider equation (2.1). For simplicity $G(\theta,\phi)$ is taken as the antenna pattern and the influence of the radiometer receiver is temporarily neglected. The problem of the smoothing action of the antenna pattern can be demonstrated by considering the following example of brightness temperature and antenna pattern:

$$T_1(\theta,\phi)= T(\theta,\phi), \quad T_2(\theta,\phi) = T(\theta,\phi) + C\cos(\omega\theta)$$

$$G(\theta,\phi)= \begin{cases} \frac{4\pi}{\Omega_a} & 0 \le \Omega \le \Omega_a \\ 0 & \text{elsewhere} \end{cases} \tag{2.4}$$

The difference between $T_{A_1} = G*T_1$ and $T_{A_2} = G*T_2$ (where $*$ denotes the integral operator) is given by:

$$|T_{A_1}-T_{A_2}| = \frac{C}{4\pi}\frac{4\pi}{\Omega_a}\int_{\Omega_a}\cos(\omega\theta)d\Omega \propto \frac{C}{\Omega_a\,\omega} \tag{2.5}$$

So, by making ω sufficiently large or C sufficiently small, the difference can become very small and it will become impossible to distinguish between T_1 and T_2. This means that integration with the antenna pattern is equivalent with low–pass filtering. This result also forms an introduction to the problems related with d). Due to the smoothing action of the antenna–pattern, small–amplitude or spatially–rapid variations in $T(\theta,\phi)$ will have no effect on T_A. Otherwise stated, a detectable change in T_A will have to come from a relatively large or slow change in $T(\theta,\phi)$. However, the antenna temperature is measured with a non–ideal radiometer receiver which introduces additional noise to the noisy signal T_A. So, a change in T_A can also originate from the radiometer receiver. Performing the inversion process in that case will lead to errors in the reconstruction of the original brightness temperature. This makes clear that the problem of inversion is a very complex matter.

The related problems originate from the physical relation as given by Eq.(2.2). These problems can not be solved by increasing the accuracy and efficiency of the numerical algorithms used in the inversion process. This is due to the fact that Eq.(2.2) is a first kind Fredholm integral which is a well–known example of an ill–posed problem; this means [6] that Eq.(2.2) does not satisfy the following properties:

1) for every T_A there exist a solution T
2) the solution T is unique
3) the problem is stable, such that a small change in T leads to a small change in T_A and vice versa.

The discussion above makes clear that the second and third properties are not satisfied, making the problem ill–posed.

Luckily, the inversion can sometimes be facilitated by assuming knowledge about object and data properties. This knowledge would exclude a large variety of solutions, that would otherwise be generated. Some examples of a–priori knowledge are: the mean and standard deviation of the noise temperature as derived from statistics, and the upper and lower limit of the noise temperature as derived from worst case statistics.

To be able to perform the inversion, a model for the radiometric measurements is needed.

2.2 Modelling the relation between the observed scene and radiometer

The basis for the modelling is formed by Eq.(2.2). Firstly, the scene is projected to a x–y plane, given by the vectors $\underline{x}$ and $\underline{y}$ (where $\underline{x}$ represents the direction of the movement), and represented by a brightness temperature distribution T(x,y). Figure 2.2 shows the coordinates used.

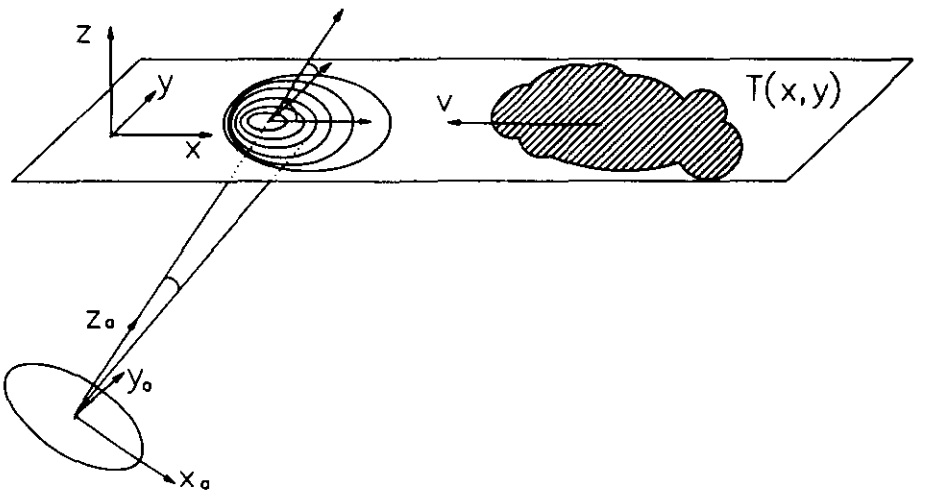

Figure 2.2. The coordinate systems.

The relative movement between the cloud and the radiometer can be modelled as the movement between the antenna contour plots on the x–y plane and the distribution T(x,y) (changing the three–dimensional problem into a two dimensional one, see figure 2.2). Due to the fact that measurements can be taken at different relative

positions between antenna and scene, it is possible to estimate T(x,y) in the direction of the movement. Indirectly, it is also possible to gain knowledge about the boundaries of the scene (in the direction of the movement) because outside the cloud T(x,y)=0 is found. At Eindhoven University of Technology (EUT) an antenna is used in a non–scanning configuration and reconstruction is only possible in the direction of the movement. Perpendicular to this direction the antenna smoothing effect can not be cancelled. Therefore it is obvious to try to convert the problem to a one dimensional problem to simplify calculations. Assuming that the movement, with constant v along the x–axis is linear in the time interval of measurements it is possible to write:

$$T_a(t) = \frac{1}{\tau}\int_{t-\frac{\tau}{2}}^{t+\frac{\tau}{2}}\left[\frac{1}{4\pi}\int_{-\infty}^{\infty}\int_{-\infty}^{\infty}\frac{T(x-v\xi,y)}{R^2(x,y)}G(x,y)dxdy\right]d\xi = \tag{2.6}$$

$$= \frac{1}{\tau}\int_{t-\frac{\tau}{2}}^{t+\frac{\tau}{2}}\left[\frac{1}{4\pi}\int_{-\infty}^{\infty}\int_{-\infty}^{\infty}\frac{T(x,y)}{R^2(x,y)}G(x+v\xi,y)dxdy\right]d\xi$$

$$T_a(t) \approx \frac{1}{\tau}\int_{t-\frac{\tau}{2}}^{t+\frac{\tau}{2}}\left[\frac{1}{4\pi}\int_{-\infty}^{\infty}T(x,Y)\int_{-\infty}^{\infty}\frac{G(x+v\xi,y)dy}{R^2(x,y)}dx\right]d\xi \tag{2.7}$$

where T(x,Y) is an average value with respect to the y–coordinate. In this way it is possible to write:

$$T_a(t) \approx \frac{1}{4\pi}\int_{-\infty}^{\infty}T'(x)G'(x,t,\tau)\,dx \tag{2.8}$$

with $T'(x) = T(x,Y)$ and $G'(x,t,\tau) = \frac{1}{\tau}\int_{t-\frac{\tau}{2}}^{t+\frac{\tau}{2}}\left[\int_{-\infty}^{\infty}\frac{G(x+v\xi,y)dy}{R^2(x,y)}\right]d\xi$

Here it is assumed that in a period τ, needed to obtain $T_a(t)$, T(x,Y) does not vary and can be taken as frozen.

The evaluation of eq.(2.8) needs some mathematical manipulation. This problem is simplified if the movement is divided into a movement parallel to the antenna aperture and a movement towards the antenna (see figure 2.3).

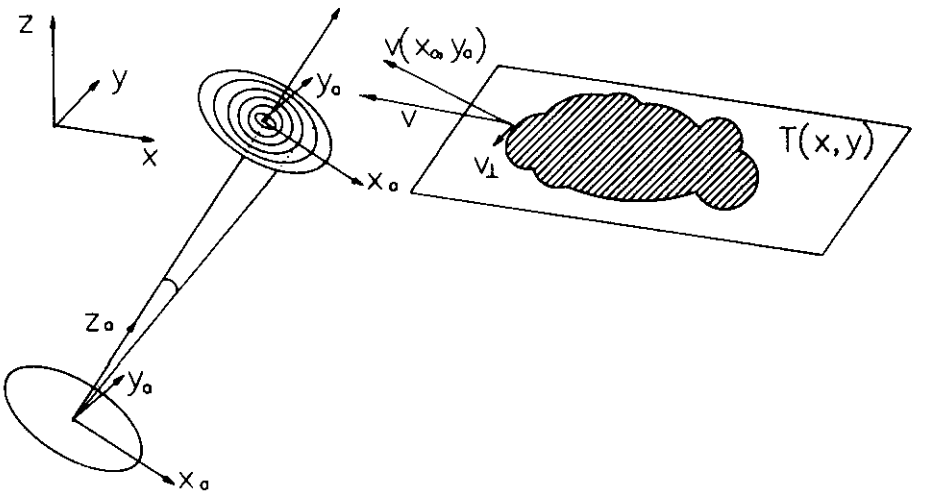

Figure 2.3. Modelling the movement.

As a change in R will be small for subsequent measurements it is possible to neglect the latter movement. In this way all the antenna–pattern symmetry properties are maintained and the mathematical manipulations are kept to a minimum.

3 Reconstruction

3.1 The estimation of T'

In the previous chapter, a model was derived for the relative movement between the scene and the radiometer system. The problem of determining T'(x) can now be dealt with in several ways [1],[2],[3],[4] but it can be visualized as in figure 3.1.

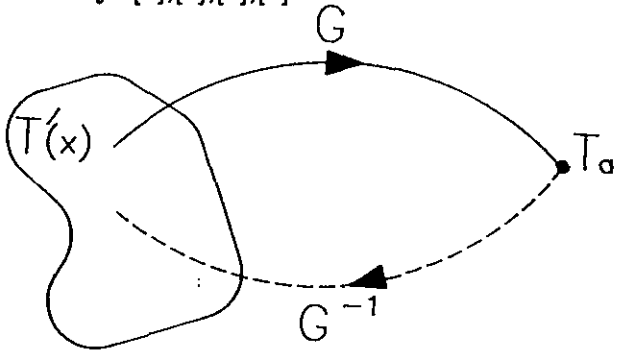

Figure 3.1. The projection of the set T'(x) to T_a

Due to the fact that the problem is ill posed, the T_a measured corresponds to a set of functions T'(x) and it is necessary to develop an inversion G^{-1} which gives an unique T'(x) as solution to the problem. Different inversions methods G^{-1} will result in a different function T'(x). However, as a radiometer system is used, it is rational to treat the imaging problem from the radiometer point of view. It is possible to draw a parallel with the traditional use of the radiometer for for accurate measurement of T_a as a function of time. In this way it is possible to obtain radiometer statistics which can be used for predicting the quality of a future satellite link. In such a radiometer system an antenna is used, followed by a highly sensitive microwave receiver which basically consists of an RF–amplifier, mixer, IF–amplifier, filter, square–law detector and an integrator. The integrator is used to improve the radiometer sensitivity which is defined as the minimum change in input signal that is necessary to produce a detectable change in the output signal. Detectable is defined as a change in dc–level of the output voltage equal to the standard deviation of the superimposed ac–signal. So, the integrator is used to get the best possible estimate of the average of the antenna brightness temperature. If T_a is written as follows:

$$T_a(t) = \langle T_a(t) \rangle + \delta T_a(t) \qquad (3.1)$$

where <.> indicates ensemble averaging, the intention is to minimize the time

variations $\delta T_a(t)$. Otherwise stated it is the intention to reconstruct the signal T_a in time.

With an imaging radiometer, where the objective is to reconstruct $T'(x)= <T'(x)> + \delta T'(x)$, it is therefore reasonable for trying to get the best possible estimate of the average of T' with respect to x, while minimizing the spatial variations $\delta T'(x)$. This can be accomplished by minimizing:

$$\int_{-\infty}^{\infty} T'^2(x)dx = <T'(x)>^2 + \int_{-\infty}^{\infty} \{\delta T'(x)\}^2 dx \tag{3.2}$$

with the constraint that T' has to satisfy the measurements given by Eq.(2.8). Here it is assumed that $\delta T'(x)$ varies rapidly with respect to the average value.
Using the following formulation:

$$T_{ai} = \frac{1}{\tau}\int_{t_i-\frac{\tau}{2}}^{t_i+\frac{\tau}{2}} T_A(\xi)\, d\xi = \frac{1}{4\pi}\int_{-\infty}^{\infty} T'(x)\, G_i'(x)\, dx \tag{3.3}$$

$$\text{with } G_i'(x) = \frac{1}{\tau}\int_{t_i-\frac{\tau}{2}}^{t_i+\frac{\tau}{2}} \left[\int_{-\infty}^{\infty} \frac{G(x+v_x\xi,y)dy}{R^2(x,y)}\right] d\xi$$

it is possible to write the problem as: reconstruct T'(x) which satisfies

$$T_{ai} = \frac{1}{4\pi}\int_{-\infty}^{\infty} T'(x)G_i'(x)\, dx \quad (1\leq i\leq N) \text{ and minimizes } \int_{-\infty}^{\infty} \{T'(x)\}^2 dx \tag{3.4}$$

Using this discretization, it is possible to transform the integral relation into a matrix equation. Eq.(3.4) can be seen as a dot product in a function space.

$$\begin{aligned} T_{a1} &= \frac{1}{4\pi} G_1' \cdot T' \\ T_{a2} &= \frac{1}{4\pi} G_2' \cdot T' \\ &\vdots \\ T_{aN} &= \frac{1}{4\pi} G_N' \cdot T' \end{aligned} \tag{3.5}$$

Furthermore T' has to minimize Eq.(3.2), which can be written as:

$$\min\{T' \cdot T'\} = \min\{ ||T'|| \} \tag{3.6}$$

Here $||T'||$ represents the "length" of T' in the function space, which can be visualized as given in fig.3.2.

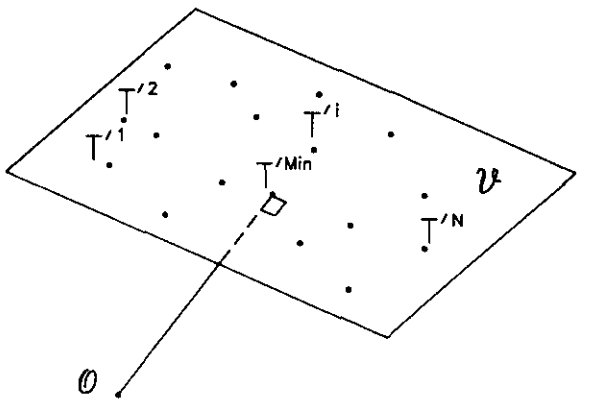

Figure 3.2. The length of T' in function space. T^i represents a T' that satisfies Eq.(3.5)

Here $\mathcal{V}$ represents a linear manifold in function space containing all the functions T' which satisfy Eq.(3.5). The solution to Eq.(3.4) is the T' which has the minimum "distance" to the origin $\mathcal{O}$. A detailed mathematical derivation and the consequences of this constraint for the form of T' is given in Appendix A, but it can easily be understood that the T' with the minimum length from $\mathcal{O}$ to $\mathcal{V}$ has to be perpendicular to $\mathcal{V}$. Using Eq.(3.5) it is clear that a T' that satisfies that condition can be written as:

$$T' = \sum_{i=1}^{N} a_i G_i' \tag{3.7}$$

$$\text{So } T_{ai} = \frac{1}{4\pi} G_i' \cdot T' \Rightarrow T_{ai} = \left(\frac{1}{4\pi}\right) G_i' \cdot \sum_{j=1}^{N} a_j G_j' \Rightarrow T_{ai} = \left(\frac{1}{4\pi}\right) G_i' \cdot \underline{G}^T \underline{a} \Rightarrow$$

$$\underline{T}_a = \left(\frac{1}{4\pi}\right) \underline{G} \cdot \underline{G}^T \underline{a} \tag{3.8}$$

or, $\underline{T}_a = G\underline{a}$ (3.9)

with $\underline{T}_a = \begin{bmatrix} T_{a\,1} \\ T_{a\,2} \\ \vdots \\ T_{aN} \end{bmatrix}$, $\underline{a} = \begin{bmatrix} a_1 \\ a_2 \\ \\ a_N \end{bmatrix}$, $\underline{G} = \begin{bmatrix} G_1' \\ G_2' \\ \\ G_N' \end{bmatrix}$ and G a N×N matrix with elements

$$G_{ij} = \left[\frac{1}{4\pi}\right] \int_{-\infty}^{\infty} G_i'(x) G_j'(x)\, dx. \qquad (3.10)$$

It is simple to determine the reconstruction vector $\underline{a}$ via:

$$\underline{a} = G^{-1}\underline{T}_a \qquad (3.11)$$

The corresponding $\underline{T}'$ can be found by substituting $\underline{a}$ in Eq.(3.7). The matrix G' is a Gramm matrix, but in this special case it is also a Toeplitz matrix which takes the form of a positive definite, symmetric band matrix with elements $G'_{i,j}=G'_{i-k,j-k}$.

3.2 Trade–off between resolution and accuracy

The above reconstruction technique enables T' to be written as a summation of shifted versions of the antenna pattern G'. As an example the process of reconstruction is illustrated in figure 3.3.

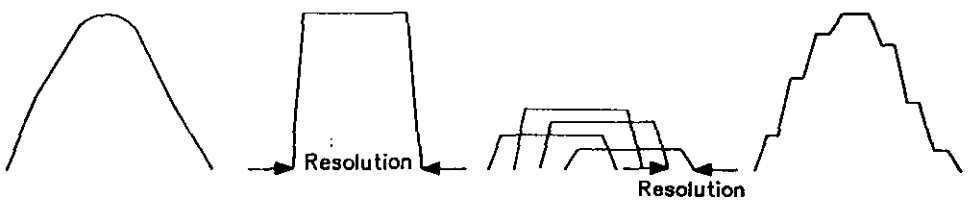

a) b) c) d)

Figure 3.3. The process of reconstruction: a)Input b) G'(x) c) $a_iG_i'(x)$ d) T'(x)

The pattern G' is given in figure 3.3.b and $G_i'(x)$ in figure 3.3.c, if N=4, a_1=0.3, a_2=0.5, a_3=0.4, a_4 = 0.2, T' will be as given in figure 3.3.d.
In terms of resolution it is desirable to have as many, slightly shifted G_i's as possible; then it is possible to reconstruct T' in more detail. However, calculating $\underline{a}$ in that case can lead to unacceptable errors in the reconstruction. If G_i' is a slightly shifted version of G_1' there will be a strong interdependence between the rows and columns of G, resulting in a large condition number of G. As T_a is contaminated with noise from the radiometer receiver, this noise can be multiplied with the condition number during the calculation of $\underline{a}$. To improve the condition number, it is necessary to make the interdependence less. This implies that there has to be as little overlap as possible. Therefore the reconstruction of T' asks for a trade–off between resolution and accuracy of reconstruction.

3.3 Measurements contaminated with noise

3.3.1 Statistical errors due to the receiver

The method derived in section 3.2 selects T' to satisfy Eq.(3.4) and it neglects a–priori knowledge of the existence of measurement errors in the signal T_a. One contributor to the measurement error is the radiometer receiver which introduces a statistical error equal to the radiometer temperature resolution ϵ. Statistical errors on the antenna pattern can be neglected because the influence is minimal due to both spatial and time integration of the pattern. Therefore, the problem as stated in Eq.(3.3) and Eq.(3.6) is more realistically represented by:

$$|| (\tfrac{1}{4\pi})\underline{G}\cdot\underline{T}' - \underline{T}_a ||^2 \leq \epsilon^2 \quad \text{and} \quad \min\{|| \underline{T}' ||\} \tag{3.12}$$

and figure 3.1 changes into figure 3.4.

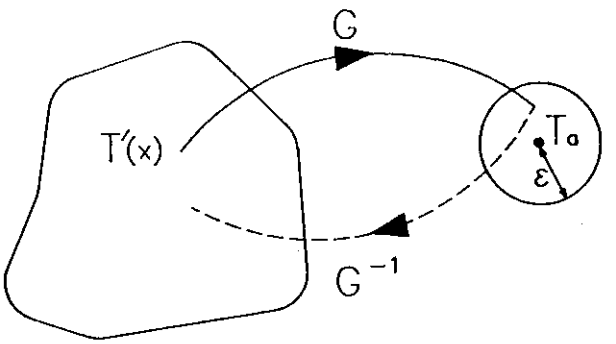

Figure 3.4. The projection of the set T'(x) to the set T_a.

The set T'(x) becomes larger and makes it possible to search for a smoother (a more "well–behaved") solution to the ill–posed problem. In Appendix A.2. it is shown that the solution to this problem can again be written as a linear combination of antenna patterns, so using Eq.(3.7), Eq.(3.12) becomes:

$$|| G\underline{a} - \underline{T}_a ||^2 \leq \epsilon^2 \qquad \text{and,} \tag{3.13.a}$$

$$\min\{(\underline{G}^T\underline{a} \cdot \underline{G}^T\underline{a})\} \Rightarrow \min\{4\pi(\underline{a}^T G\underline{a})\} \tag{3.13.b}$$

where ϵ is the radiometer temperature sensitivity.
In Appendix B it is shown that this problem is equivalent with:

$$|| G\underline{a} - \underline{T}_a ||^2 = \epsilon^2 \qquad \text{and,} \tag{3.14.a}$$

$$\min\{4\pi(\underline{a}^T G\underline{a})\} \tag{3.14.b}$$

With the help of the Lagrange multipliers it is possible to show that the solution to this problem has to satisfy:

$$2G\underline{a} = \text{grad}(\underline{a}^T G\underline{a}) = a\ \text{grad}(||G\underline{a} - \underline{T}_a||^2) = a(2G^T G\underline{a} - 2G\underline{T}_a) \tag{3.15}$$

Noting that G is positive definite and $G^T = G$, it follows that:

$$\underline{a} = a(G\underline{a} - \underline{T}_a) \tag{3.16}$$

So the problem becomes:

$$|| G\underline{a} - \underline{T}_a ||^2 = \epsilon^2 \qquad \text{and,} \qquad (3.17.a)$$

$$\underline{a} = a(G\underline{a} - \underline{T}_a) \qquad (3.17.b)$$

From Eq.(3.17.a) it follows that:

$$G\underline{a} = \underline{T}_a - \epsilon^2\underline{z} \quad \text{with } ||\underline{z}||^2 = 1 \qquad (3.18)$$

Substitution of 3.18 in Eq.(3.17.b) gives:

$$\underline{a} = a(\underline{T}_a - \epsilon^2\underline{z} - \underline{T}_a) = -a\epsilon^2\underline{z} \qquad (3.19)$$

or,

$$a\epsilon^2\underline{z} = a(Ga\epsilon^2\underline{z} + \underline{T}_a) \Rightarrow \epsilon^2(I - aG)\underline{z} = \underline{T}_a \Rightarrow (I - aG)^{-1}\underline{T}_a = \epsilon^2\underline{z} \qquad (3.20)$$

$$\Rightarrow ||(I - aG)^{-1}\underline{T}_a||^2 = \epsilon^2 \qquad (3.21)$$

So, after calculating a from Eq.(3.21) it is possible to derive $\underline{a}$ from Eq.(3.17.b).

However, the problem as given by Eq.(3.21) is not linear anymore and the solution is not that straightforward. One way to determine a is based on diagonalization of the Gramm matrix G:

$$G = BDB^T \qquad (3.22)$$

with D a diagonal matrix with elements given by the eigenvalues $(\lambda_1, \lambda_2, .., \lambda_N)$ of the matrix G, and B an orthogonal matrix which columns are formed by the eigenvectors $(\underline{e}_1, \underline{e}_2, .., \underline{e}_N)$ of G. Furthermore, $\underline{a}$ and $\underline{T}_a$ are decomposed into the eigenvectors of the matrix G:

$$\underline{a} = \sum_{i=1}^{N} \xi_i \underline{e}_i \qquad \underline{T}_a = \sum_{i=1}^{N} \tau_{ai} \underline{e}_i \qquad (3.23)$$

leading to:

$$G\underline{a} = \sum_{i=1}^{N} \xi_i \lambda_i \underline{e}_i \qquad (3.24)$$

and Eq.(3.17.a) becomes:

$$\xi_i = a\,(\lambda_i \xi_i - \tau_{ai}) \tag{3.25}$$

and Eq.(3.20) becomes:

$$\sum_{i=1}^{N} \left(\frac{-\tau_{ai}}{1-a\lambda_i}\right)^2 = \epsilon^2 \tag{3.26}$$

This is a quadratic form in a, so two solutions will be found. To determine which a is correct, Eq.(3.17.a) is written as follows:

$$\sum_{i=1}^{N} (\lambda_i \xi_i - \tau_{ai})^2 = \epsilon^2 \tag{3.27}$$

This shows that Eq(3.17.a) is an ellipsoide. Using the sketch as shown in figure 3.5, where n represents the normal of the ellipse, it can be seen that the a that corresponds to the minimum length will be negative. The value that corresponds to the maximum length is positive. So checking the signs will give the correct a.
Substitution of a, obtained from Eq.(3.26), in Eq.(3.25) and the result in Eq.(3.23) gives the coefficients a_i and the solution to the original inversion problem.

In this way a method is obtained for regularization of the ill–posed problem. Applying the same way as described above for the case where errors are neglected (section 3.2) would have led to:

$$\underline{a} = \sum_{i=1}^{N} \frac{\tau_{ai}}{\lambda_i} \underline{e}_i \tag{3.28}$$

while the solution now takes the form of

$$\underline{a} = \sum_{i=1}^{N} \frac{-a\tau_{ai}}{(1-a\lambda_i)} \underline{e}_i \tag{3.29}$$

A small value for λ_i in Eq.(3.28) can lead to unacceptable errors in the reconstruction, while in Eq.(3.29) where a limited error is accepted this will have much less influence.

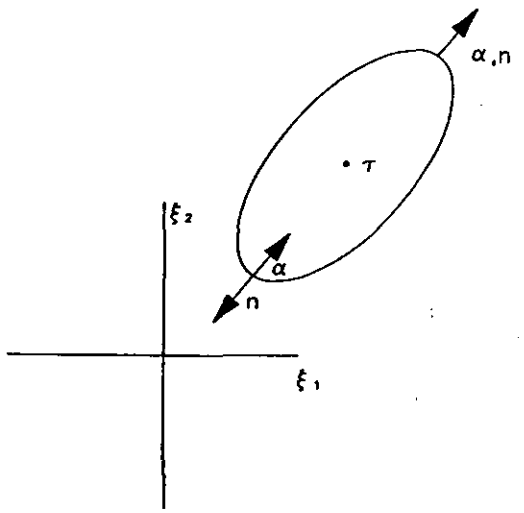

Figure 3.5. The determination of the correct a

3.3.2 Systematic errors due to the antenna

In the previous section a statistical error was discussed and in this section systematic errors are considered. Systematic errors from the receiver are neglected because they can be seen as an offset voltage which can be compensated by calibration. Systematic errors originating from the finite measurement accuracy of the antenna pattern can be shown to have little influence. This is shown in detail in Appendix C, but as can easily be seen from Eq.(3.17.b) and Eq.(3.21) the problem of determining a and $\underline{a}$ is well conditioned if the matrix G has a good condition number. So, the influence of these systematic errors is less prominent than the influence of statistical errors on the inversion method.

3.3.3 Systematic errors due to the object

In the previous section errors due to the receiver system were discussed. A short derivation in appendix D shows that incorrect estimation of the velocity of the object results in errors of the matrix G. This was to be expected from Eq.(3.3) and Eq.(3.10). Interesting to note is that the error in the G increases if the total observation time t_i increases. This is trivial if the relation $x = vt$ is considered. So, errors in v can be dealt with as discussed in the previous section and appendix C.

4 Objectives and implications

4.1 Introduction

To be able to provide relevant information about the atmospheric processes it is necessary to have some general knowledge about the scales involved in these processes. The time scales involved are important because reconstruction of the atmospheric "object" is only relevant if between successive measurements the structure can be considered as being frozen.
Knowledge of the spatial scales is important because this will define the desired resolution needed during the reconstruction.

4.2 Scales involved

The dynamic atmospheric processes range from very small–scale and rapid physical processes (the nucleation and growth of cloud particles) up to the very large–scale and slowly varying processes that are associated with synoptic weather systems. A generally adopted subdivision is that of Orlanski [7] (see figure 4.1). In figure 4.1 the relation between spatial and time extent is visible. If the smallest scale processes are omitted, it is clear from figure 4.1 that the resolution has to be in a spatial range from several meters to 20m and a time range from several seconds to 1 minute. To be able to determine the lower limit of the corresponding atmospheric processes (plumes (of clouds or from chimneys)), roughness and atmospheric turbulence) more accurate, some results of groups of meteorologists are presented.

4.2.1 Spatial extent

An impression about the spatial scales involved can be obtained from [8,9]. Here the liquid water mixing ratio is measured (see figure 4.2). In [9,pp341] it is stated that the measurements were performed with a resolution of nearly 10m and that the sharp gradients in the measurements were of a larger scale.
Another group of meteorologists [10] observed the characteristics of eddies in boundary layer cumuli. They obtained good results with a resolution of 5–10m [9,pp426] (see figure 4.3).

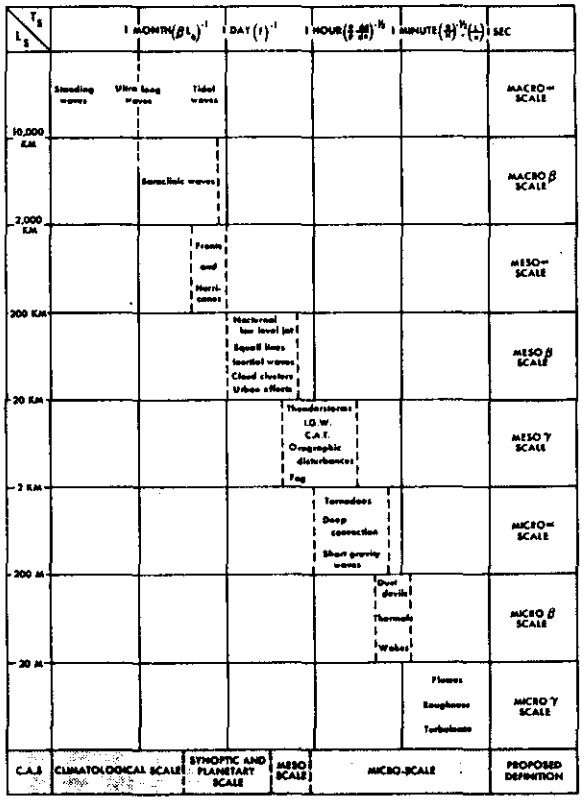

Figure 4.1. Scale definitions and different processes with characteristic time and horizontal scale.

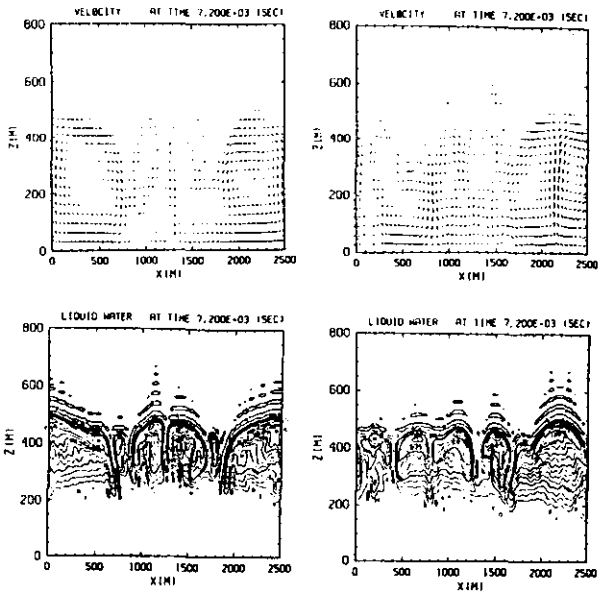

Figure 4.2. Liquid–water mixing ration at two different times. Shown are the liquid water–fields. The mixing ratio (in g kg^{-1}) is scaled by 10^3.

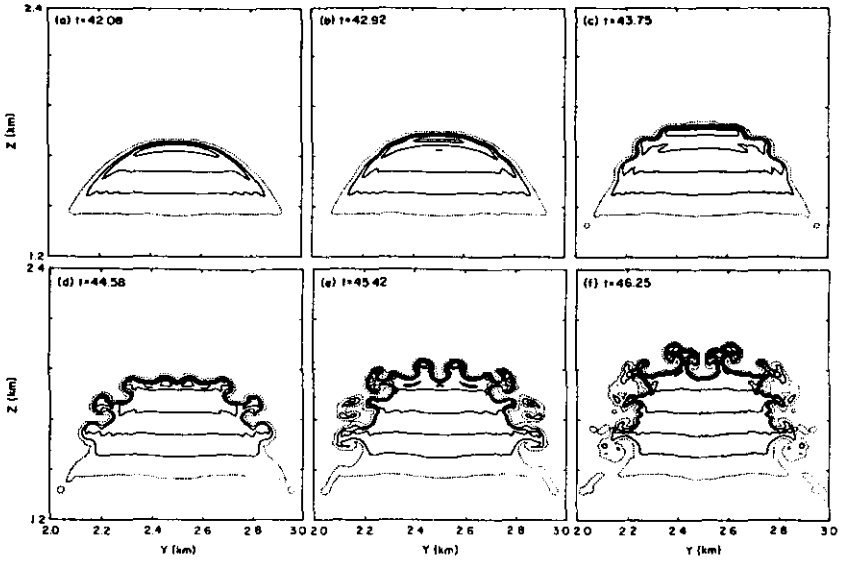

Figure 4.3. Dynamic processes in cumuli (the liquid water mixing ratio). The contour interval is 0.2 g kg^{-1} and the 0.01 contour is shown as a dotted line. The time is in minutes.

Therefore it is concluded that a resolution of 5–20m is sufficient for obtaining relevant information about atmospheric dynamics.

4.2.2 Time dependence

From figure 4.1 it is clear that the time variations are of the order of seconds to minutes. Combination of [9] and figure 4.4 [11] gives confirmation to this assumption. Taking the worst case $\frac{\Delta \text{Brightness}}{\Delta \text{Cloud thickness}}$ from figure 4.4, assuming that measurements are performed with an accuracy of 0.1K and taking the average up drift speed from [9] it is concluded that for stratus, stratocumulus and cumulus clouds it will take more than 10 seconds to measure a change.

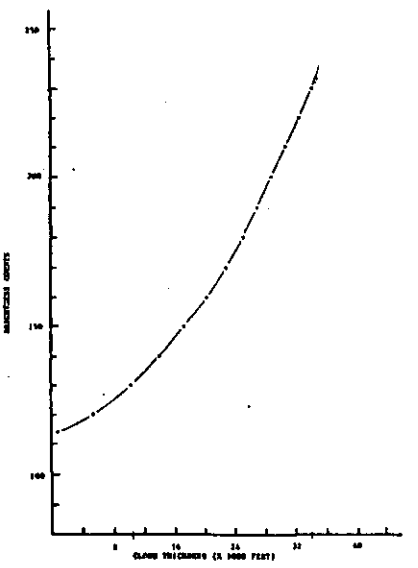

Figure 4.4. The relation between brightness and cloud thickness.

Therefore, it is concluded that for most atmospheric processes it is valid to take the structure as frozen for about 10–60 seconds.

5 Performance of the reconstruction algorithm

5.1 The antenna pattern

A skeletal structure for the reconstruction algorithm has been given in Chapter 3. Flow diagrams of the algorithm are given in appendix E. In this chapter results obtained with the algorithm are given. The first antenna pattern that is used to get a first impression of the performance is the pattern of a front–fed parabolic antenna which can be modelled adequately by a function of the following form:

$$G(\theta) = G_0 \left[\frac{J_1(a\theta)}{a\theta}\right]^2 \frac{1}{1+(a\theta)^b} \qquad (5.1)$$

(see figure 5.1.a) where a and b determine the beamwidth and level of first sidelobe, respectively and G_0 is a normalization constant.
The second pattern that is used is the pattern of a defocused parabolic antenna (see figure 5.1.b). For sake of simplicity the main lobe is approximated by the idealized pattern as given in figure 5.1.c. The reason for this is purely academic because in this way the effect of the values θ_a and θ_b (see figure 5.1.c) on the results can be determined more easily.
The defocused pattern is included because it is possible that shaping of the main lobe could affect the trade–off between resolution and accuracy of reconstruction (refer to section 3.2).

5.2 Results obtained with the approximated pattern of a front–fed antenna system

First the results of the algorithm using the pattern given by Eq.(5.1) are given. This pattern is tranformed into the G(x) pattern (the pattern after integration over the y–coordinate, see figure 5.2) followed by time averaging given by Eq.(2.8) (see figure 5.2) resulting in the G'(x) pattern.
For the examples to follow a configuration is used with a=2.6 and b=0 which is an approximation of a paraboloid of 25 λ diameter with a first sidelobe at –17.6 dB. This pattern gives a footprint of 47 m at a height of 0.5 km if the elevation angle is 90^0. The integration time of the receiver is set on 1 sec, which is representative for actual radiometers. Results are shown for different values of the resolution, which is defined as the dimension of variation that can be reconstructed (refer to section 3.2).

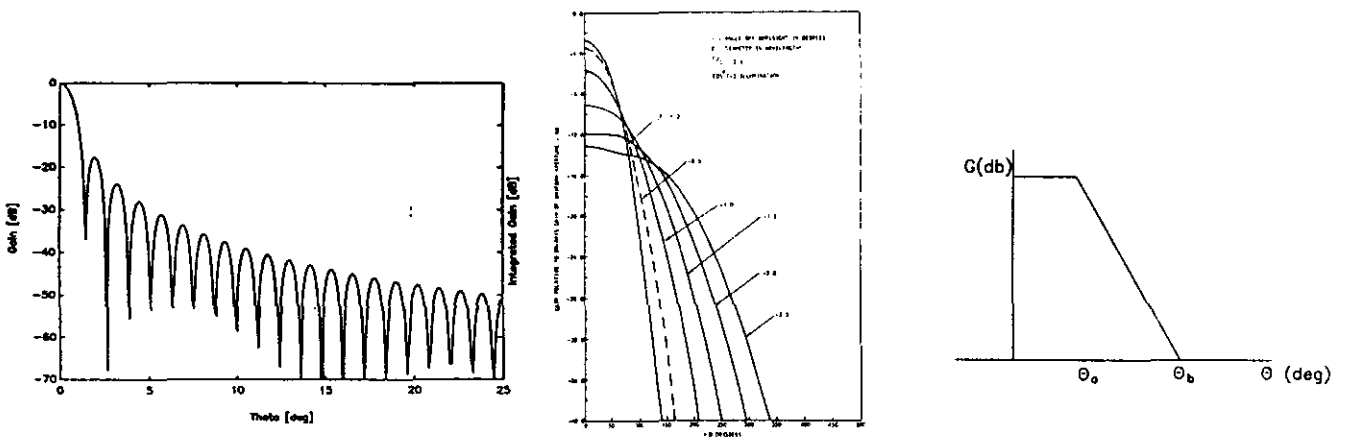

a) b) c)

Figure 5.1. The antenna patterns used in the reconstruction.

a) the pattern of a front–fed parabolic antenna system

b) the pattern of an axially defocused parabolic antenna system

c) the approximated pattern of a defocused antenna system.

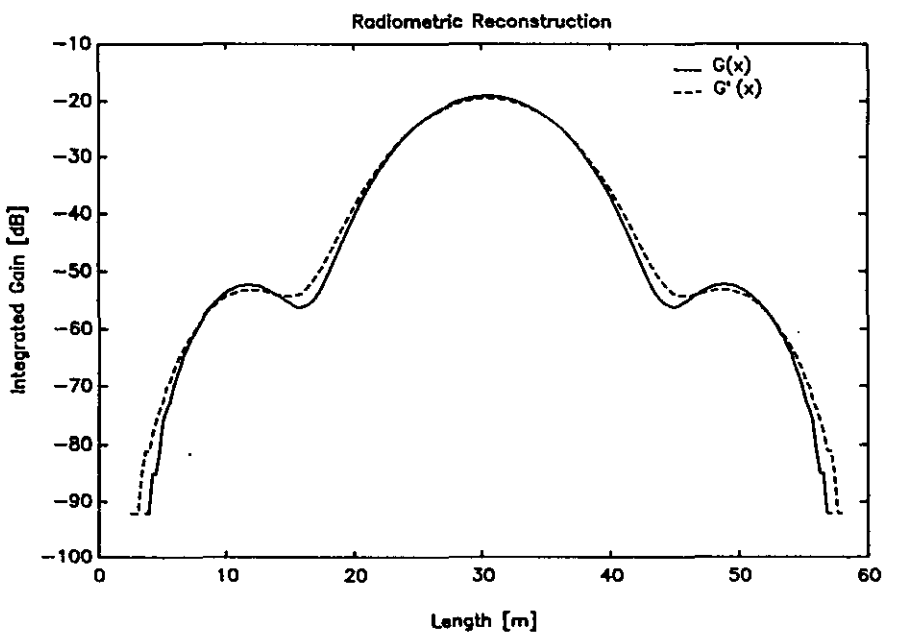

Figure 5.2.G(x) (=G(x,y) averaged over y) and G'(x) (=G(x) averaged over time).

The first example input–object is a Dirac δ–pulse. As can be seen in figure 5.3 the reconstructed signal resembles a sinc–signal, with its first zero at a distance nearly equal to the resolution. This can also be seen in figure 5.4 where the resolution is set to 15m in contrast to 6m with figure 5.3. This implies that the algorithm has a nearly rectangular spatial transfer function.

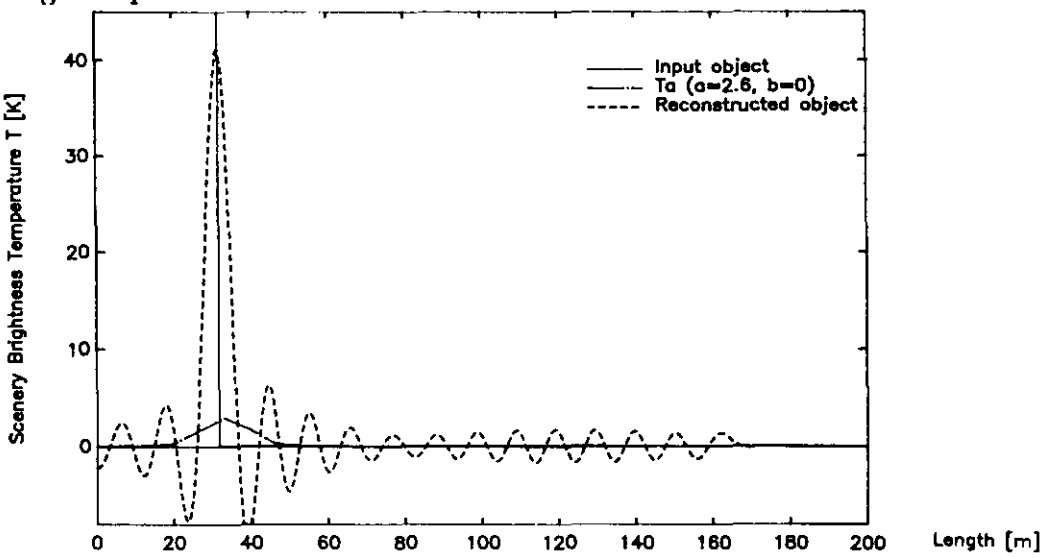

Figure 5.3. A Dirac δ–pulse input signal. The resolution is 6m.

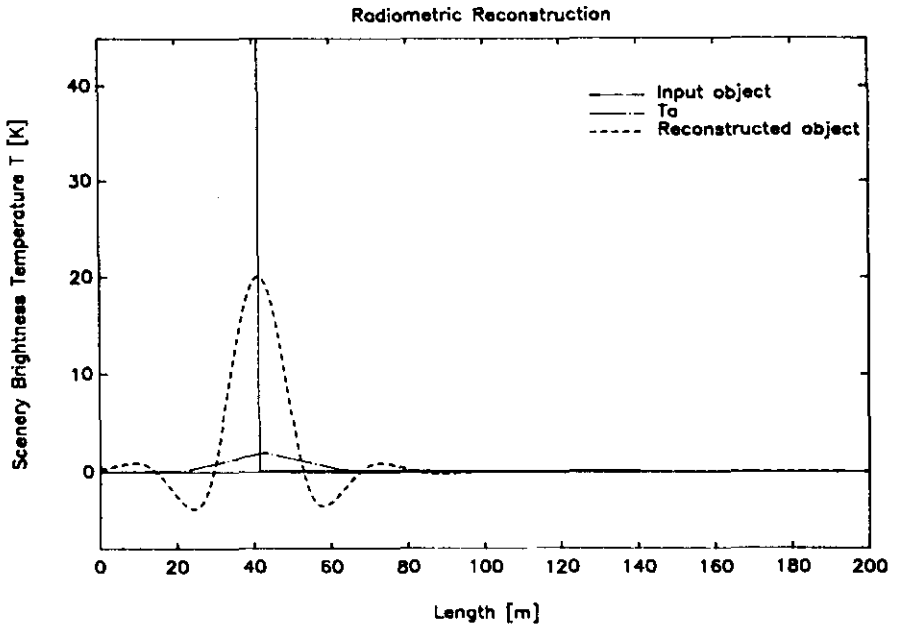

Figure 5.4. A δ–pulse input signal. The resolution is 15m.

The second input object is a sine–shaped signal. The reconstructed signal in figure 5.5 nearly equals the input signal. The reason for this extremely good result is that a sine–function is an eigenfunction of the algorithm (due to the nearly rectangular spatial transfer function).

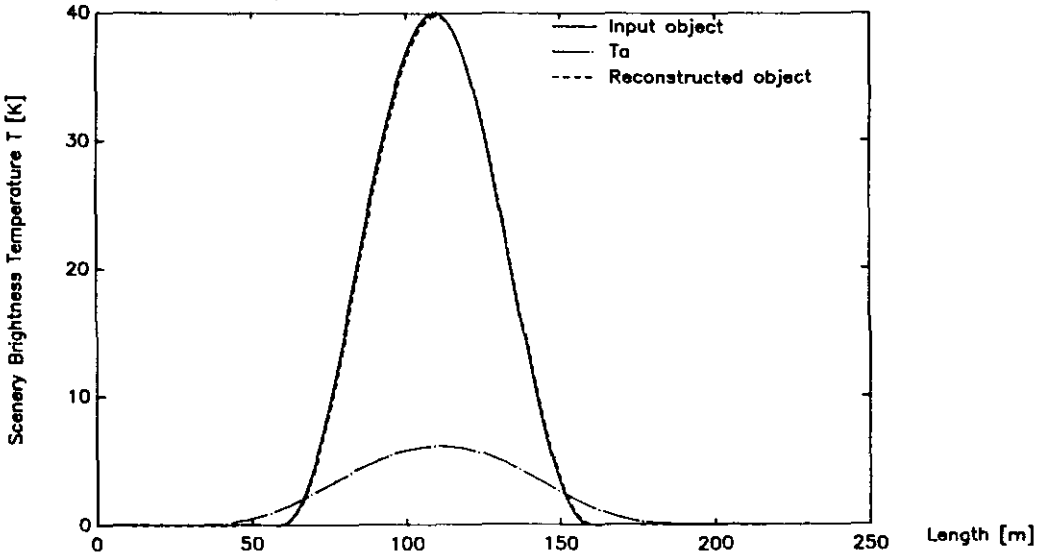

Figure 5.5. A sine–shaped input signal. The resolution is 5m.

A good example of the gain in resolution which can be obtained with this method is shown in the third example input–object. Figure 5.6 shows the result if the resolution is 15m. Figure 5.7 corresponds to a resolution of 5m. These figures clearly show the increase in resolution that is obtained with this method.

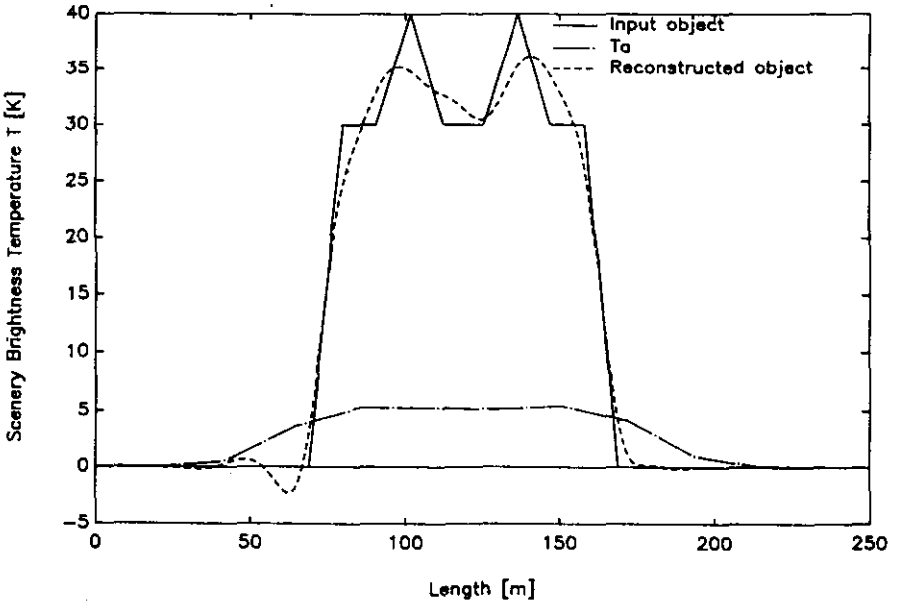

Figure 5.6. A combination of triangles as input signal. The resolution is 15m.

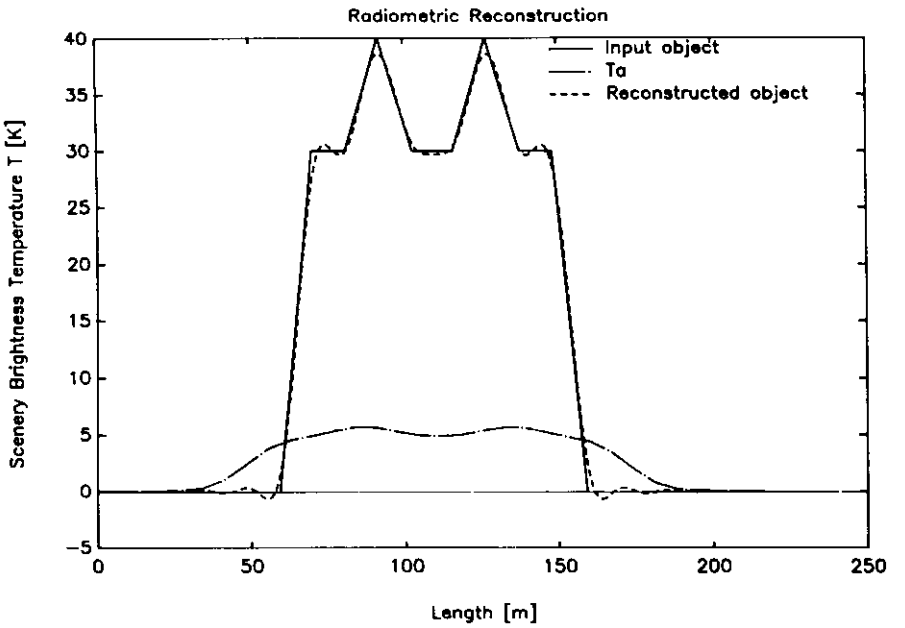

Figure 5.7. A combination of triangles as input signal. The resolution is 5m.

Finally a pulse–shaped input–signal and its corresponding reconstructed signal is shown in figure 5.8.

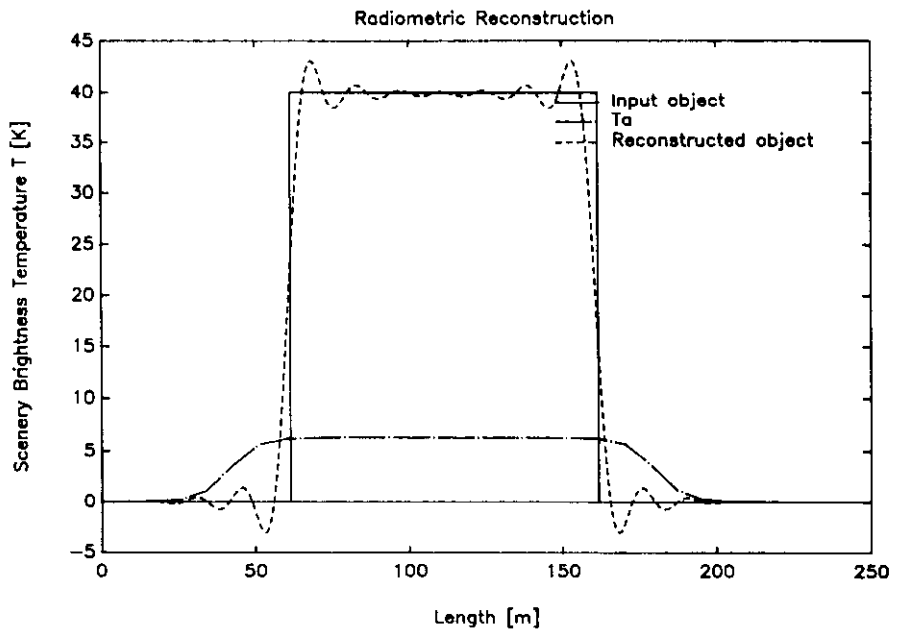

Figure 5.8. A pulsed input signal. The resolution is 5m.

5.2.1 The Influence of measurement errors in T_a

As stated previously measurement errors due to the radiometer receiver can result in a completely erroneous reconstruction of the object. In this part the signal T_a is obscured with a random noise of 0.1 K (equal to the radiometer sensitivity). If the reconstruction is based on Eq.(3.12) and the ϵ is taken as 10^{-8} (so defining the corrupted signal as exact) the reconstruction fails (see figure 5.9). If however the ϵ is taken equal to 0.1 K the reconstruction will assure good results even with noisy data (see figure 5.10).

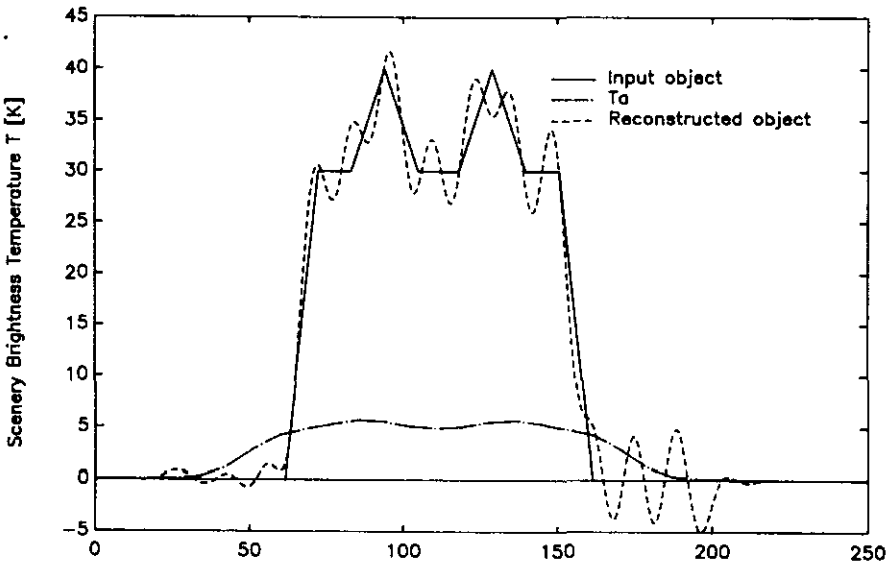

Figure 5.9. A combination of triangles as input signal. The $\epsilon = 10^{-8}$.

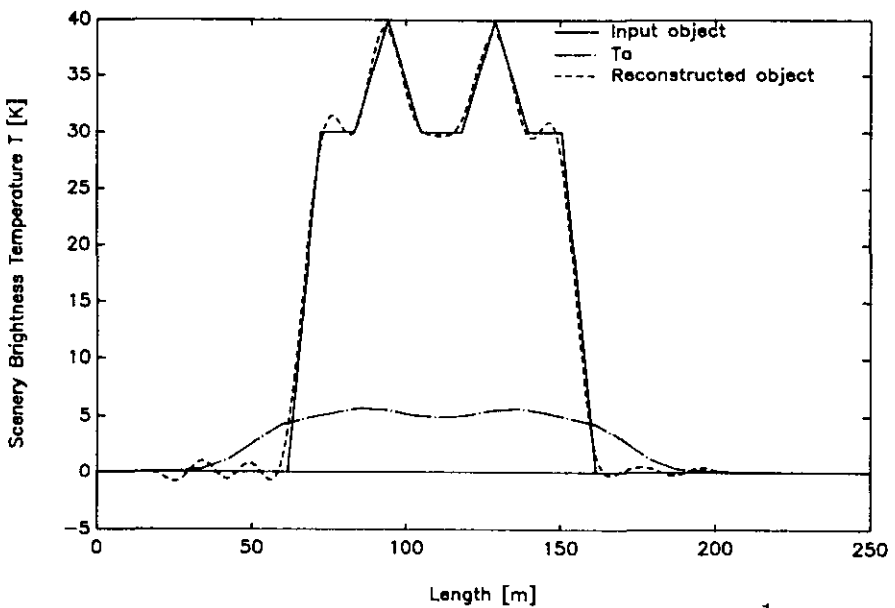

Figure 5.10. A combination of triangles as input signal. The $\epsilon = 10^{-1}$.

5.2.2 The influence of measurement errors in G

The first kind of measurement error in G that is simulated is a random error. In this section the convolution is performed with G as defined by Eq.(5.1) but the reconstruction is performed with G + random noise. The random signal is placed in a band G_{noise} around G. As can be seen in figure 5.11 the effect is of minor importance if the noise band is 2 dB. In figure 5.12 the noise band is 9 dB and the effect is clearly visible. In practice it appears that if the noise band is larger than 7 dB the reconstructed signal becomes obscured and it is clear that the effect of statistical errors can be neglected. The reason for this is that the influence is minimal due to both spatial and time integration of the pattern.

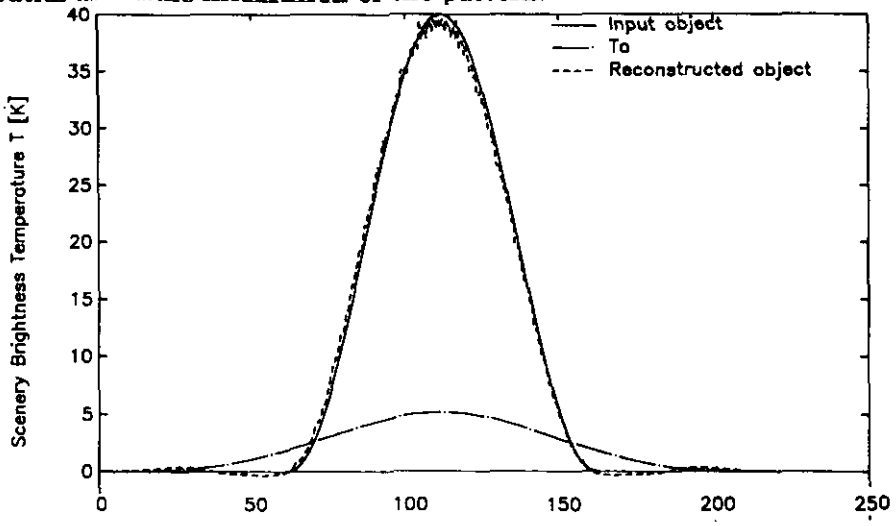

Figure 5.11. Random noise is added to the antenna pattern. G_{noise} = 2 dB.

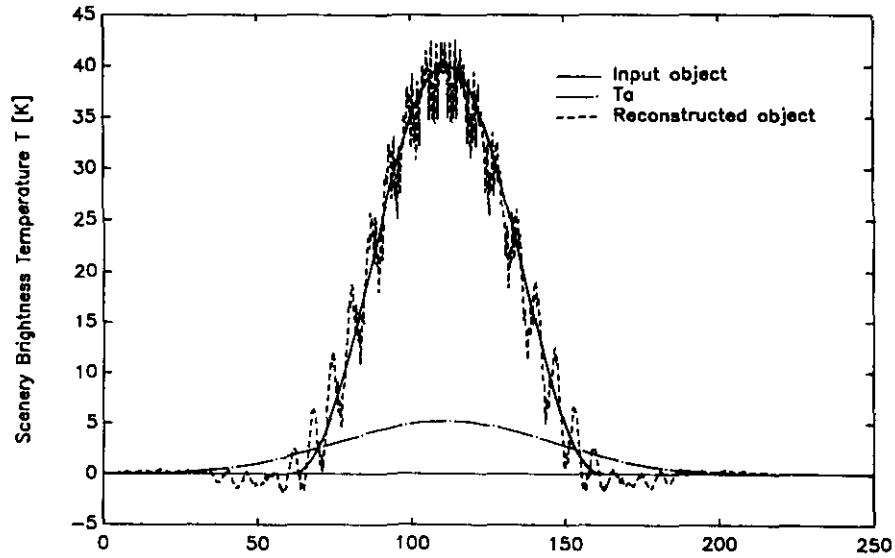

Figure 5.12. Random noise is added to the antenna pattern. G_{noise} = 9 dB.

Another error that is simulated is a systematic error in G. Now the signal T_a is determined with G as defined in Eq.(5.1) but the reconstruction is performed with a G where the parameters a and b are altered. This error could simulate a antenna pattern mismatch resulting from incorrect measurement in an antenna test range. Figures 5.13 to 5.15 show the effect for various combinations of a and b.

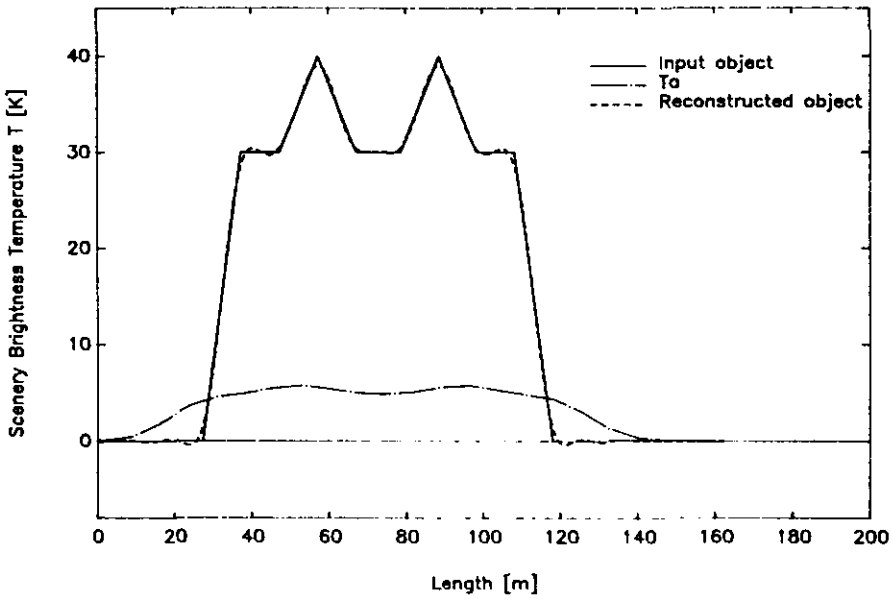

Figure 5.13. Ta determined with a=2.2, b=0. While the reconstruction is performed with a=1.1×2.2 and b=0.

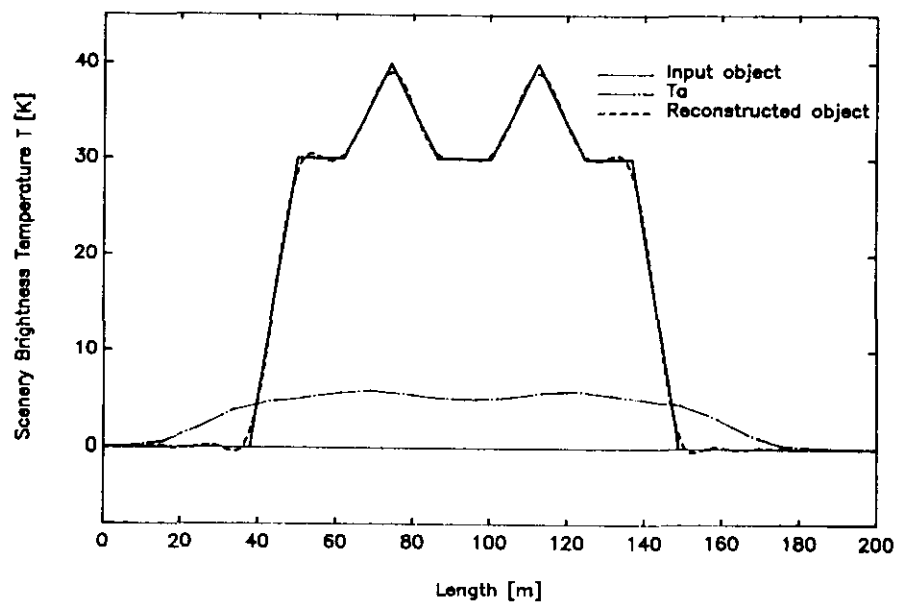

Figure 5.14. Ta determined with a=2.2, b=0. While the reconstruction is performed with a=0.9×2.2 and b=0.

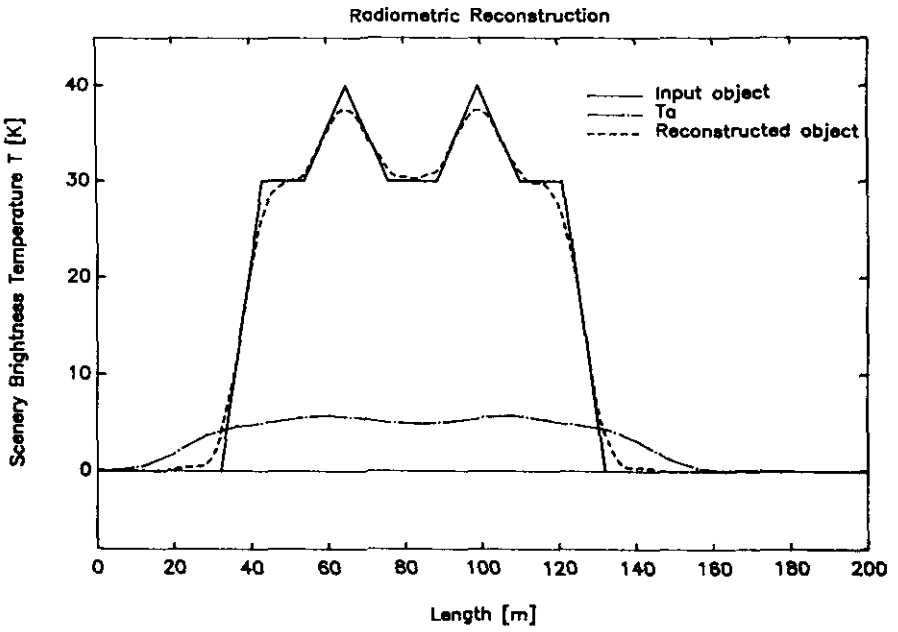

Figure 5.15. Ta determined with a=2.2, b=0. While the reconstruction is performed with a=2.2 and b=2.

These figures show that the reconstruction technique is rather insensitive for changes in the parameter a, viz. the θ–scaling of the pattern. As expected, the value of b, representing the sidelobe level, has more influence. Here b=1 corresponds to a sidelobe level of –22.4 dB.

5.3 Results obtained with the approximated pattern of a defocused antenna system

In this section results of the algorithm using the approximated pattern of a defocused antenna system are given. For the following examples θ_a and θ_b are chosen to approximate an defocused antenna system where the feed is axially displaced from the focal point of the antenna over a distance -2λ and their values are $\theta_a = 1^0$ and $\theta_b = 3^0$. The corresponding patterns G(x) and G'(x) are shown in figure 5.16.

To facilitate comparison between the results obtained with the pattern of a focused and a defocused antenna system, the same input signals as in section 5.2 are considered.

The first example input–object is again a Dirac δ–pulse. As can be seen in figure 5.17 the reconstructed signal resembles a sinc–signal, with its first zero at a distance equal to the resolution. This can also be seen in figure 5.18 where the resolution is set to 15m in contrast to 6m with figure 5.17.

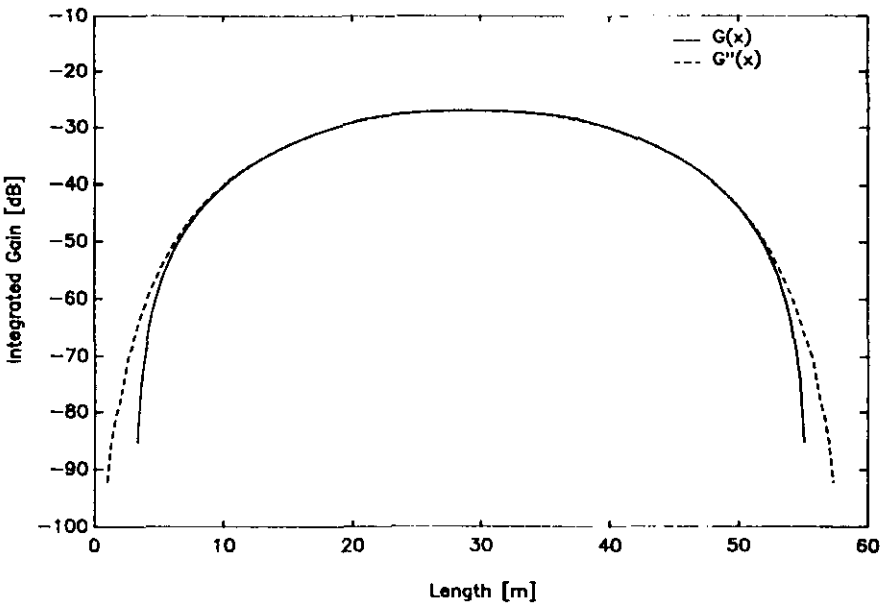

Figure 5.16. G(x) (=G(x,y) averaged over y) and G'(x) (=G(x) averaged over time).

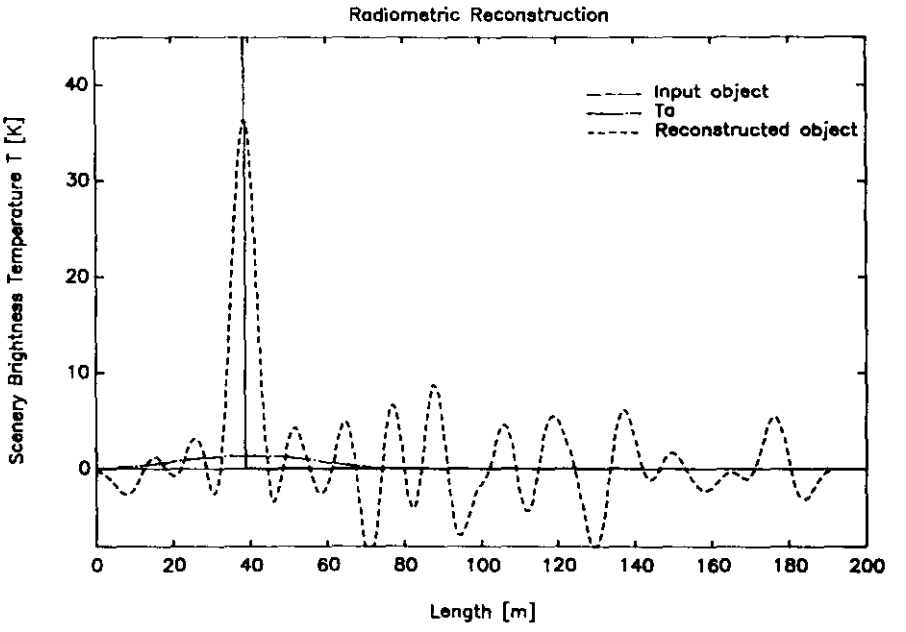

Figure 5.17. A Dirac δ–pulse input signal. The resolution is 6m.

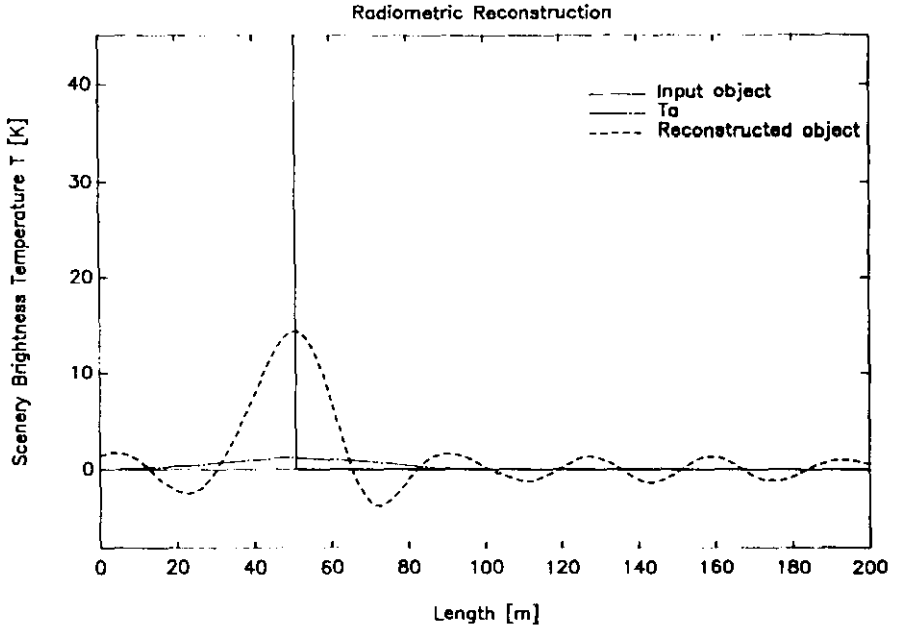

Figure 5.18. A Dirac δ–pulse input signal. The resolution is 15m.

The second input object is a sine–shaped signal. As expected the reconstructed signal in figure 5.19 nearly equals the input signal.

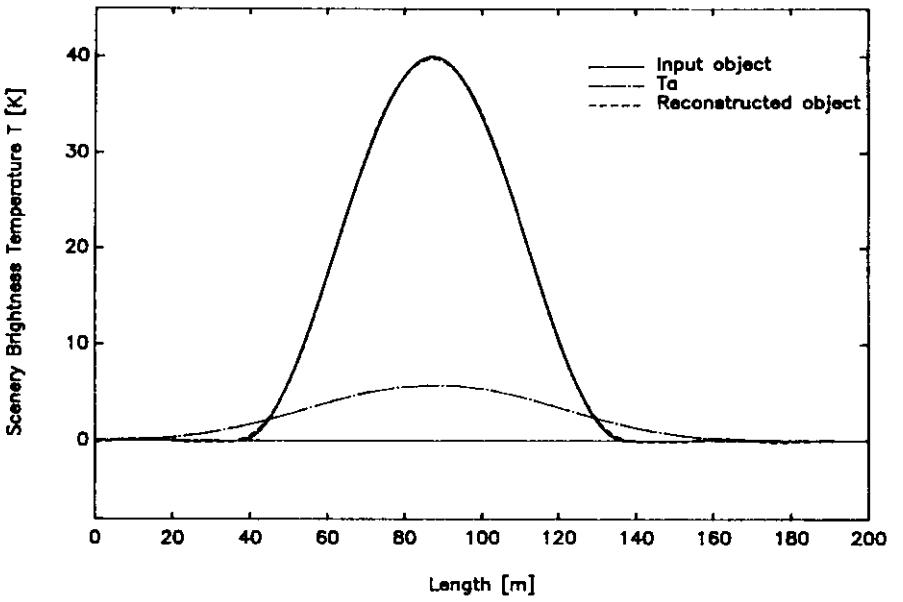

Figure 5.19. A sine–shaped input signal. The resolution is 5m.

The third example input–object is shown with a resolution of 15 m (fig. 5.20) and 5m (fig 5.21). Again the gain in resolution is clearly visible.

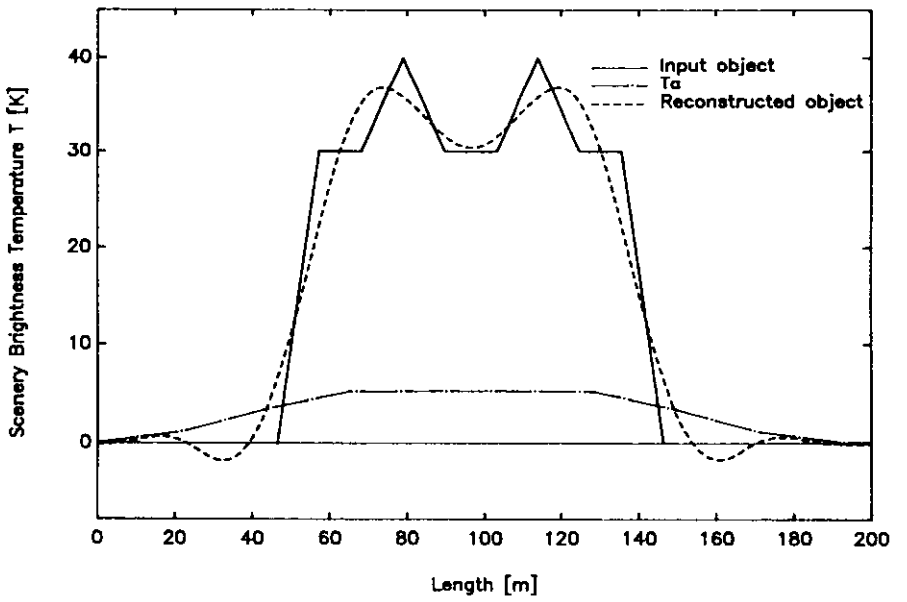

Figure 5.20. A combination of triangles as input signal. The resolution is 15m.

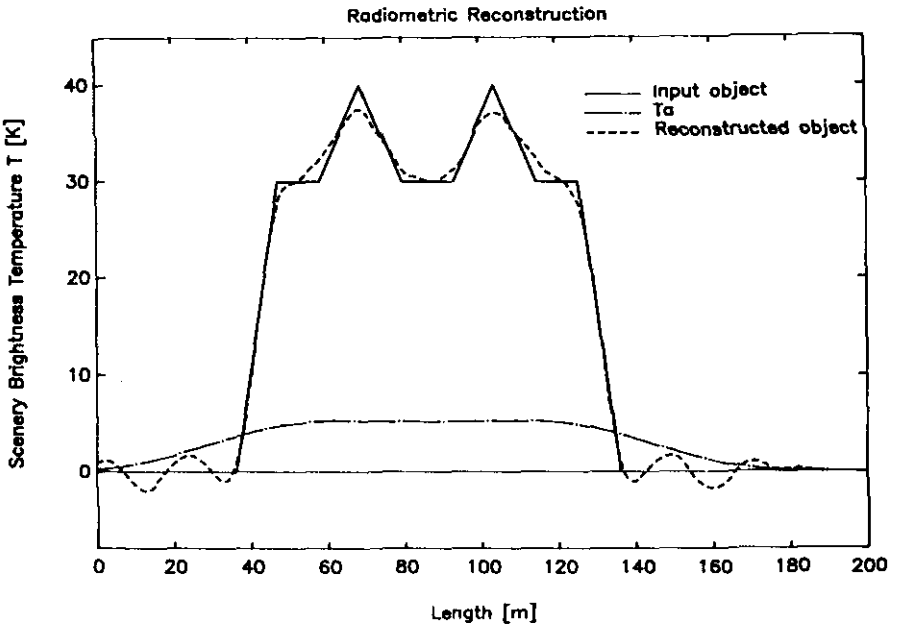

Figure 5.21. A combination of triangles as input signal. The resolution is 5m.

Finally a pulse–shaped input–signal and its corresponding reconstructed signal is shown in figure 5.22.

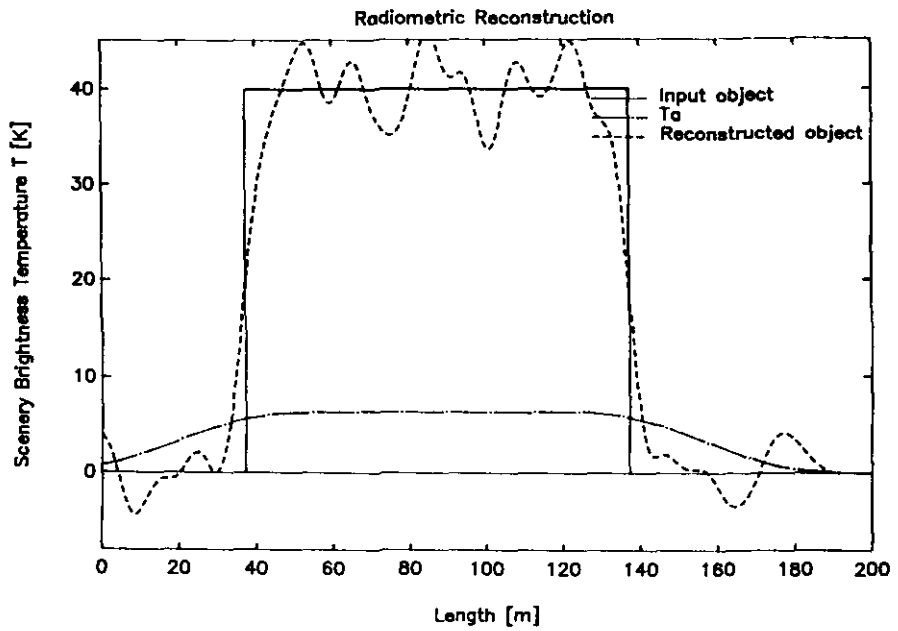

Figure 5.22. A pulsed input signal. The resolution is 5m.

5.3.1 The Influence of measurement errors in T_a

In this section the signal T_a is obscured in the same way as described in section 5.2.1 If the ϵ is taken equal to the radiometer sensitivity the reconstruction will assure good results even with noisy data and a defocused antenna pattern (see figures 5.23 and 5.24).

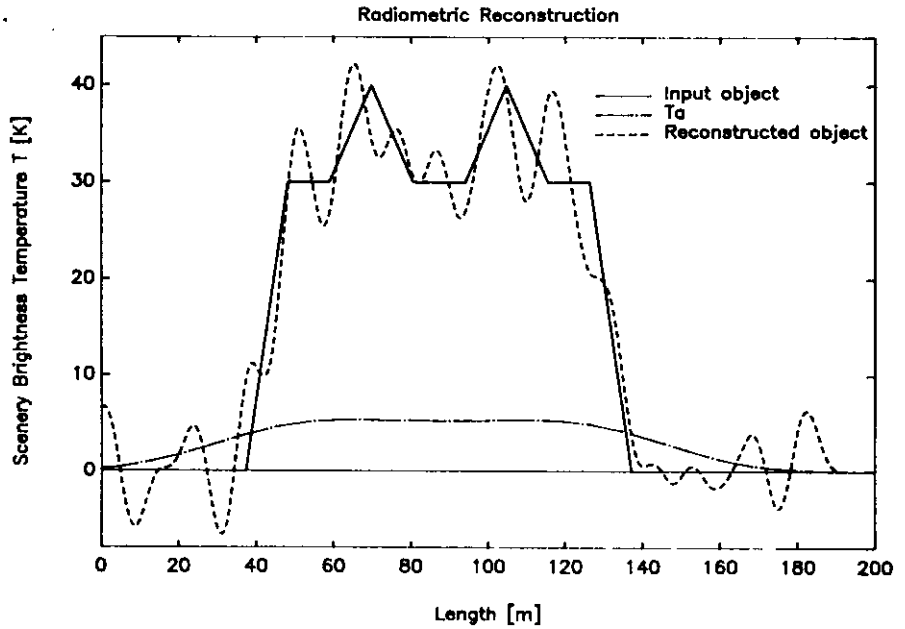

Figure 5.23. A combination of triangles as input signal. The $\epsilon = 10^{-8}$.

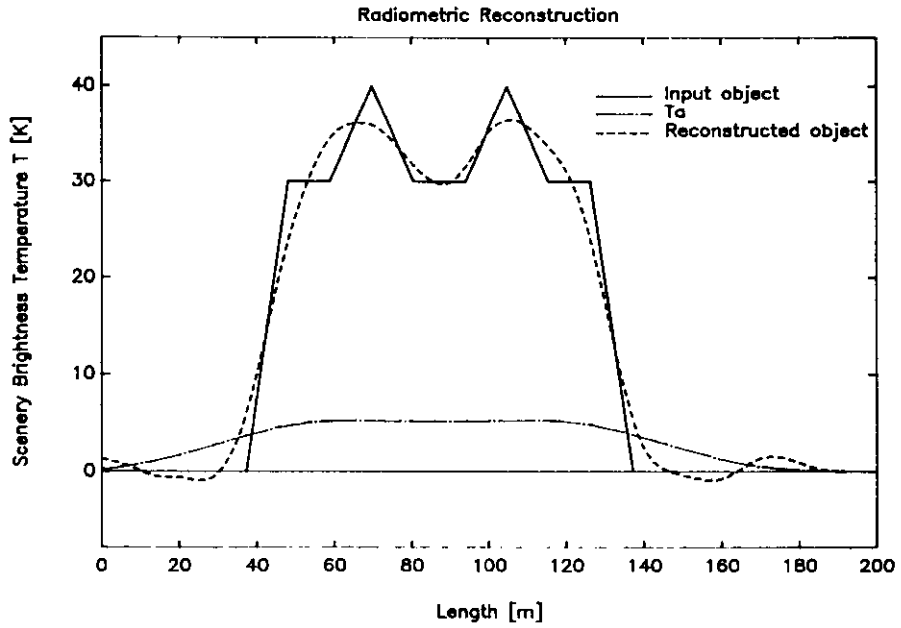

Figure 5.24. A combination of triangles as input signal. The $\epsilon = 10^{-1}$.

5.3.2 The influence of measurement errors in G

In this section the convolution is performed with G as defined in section 5.3, but the reconstruction is performed with a G where the parameters θ_a and θ_b are altered. Only this systematic error is considered, because the influence of statistical errors can be neglected. Figures 5.25 to 5.28 show the effect for various combinations of θ_a and θ_b.

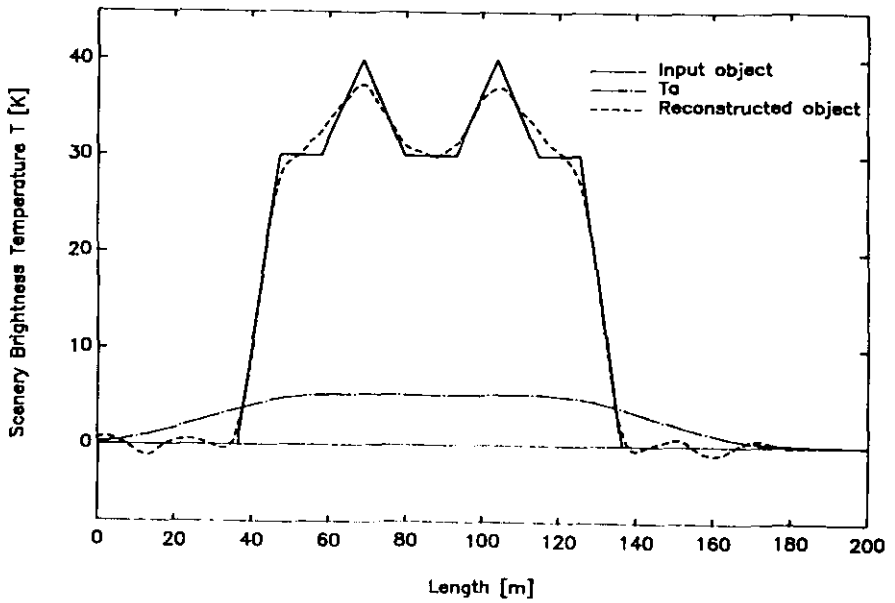

Figure 5.25. Ta determined with θ_a=1, θ_b=3. While the reconstruction is performed with θ_a=1.1×1 and θ_b=3.

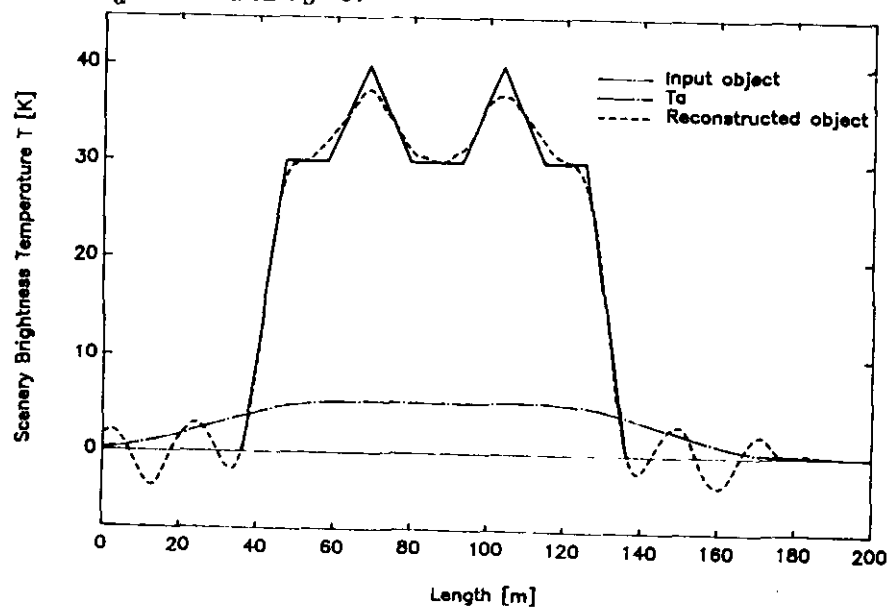

Figure 5.26. Ta determined with θ_a=1, θ_b=3. While the reconstruction is performed with θ_a=0.9×1 and θ_b=3.

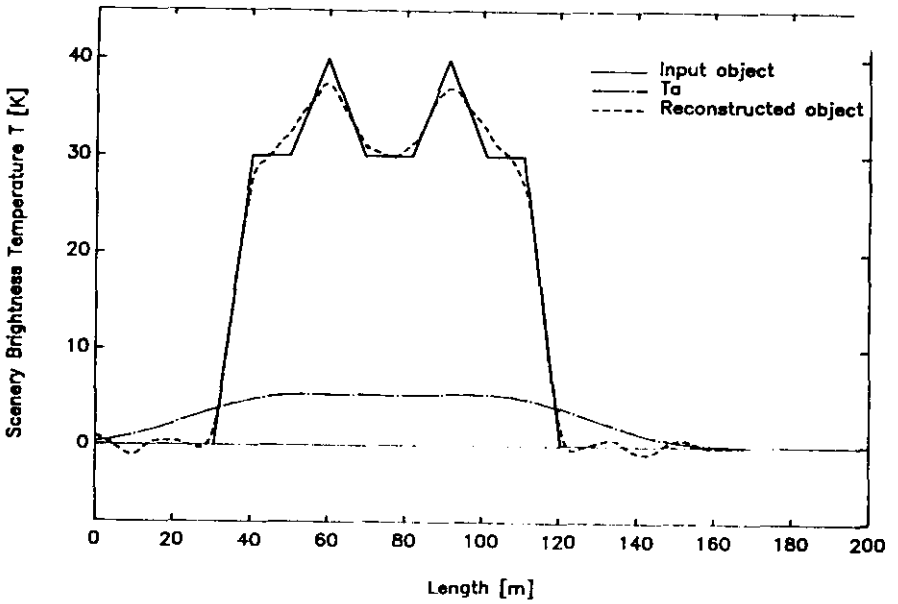

Figure 5.27. Ta determined with θ_a=1, θ_b=3. While the reconstruction is performed with θ_a=1 and θ_b=0.9×3.

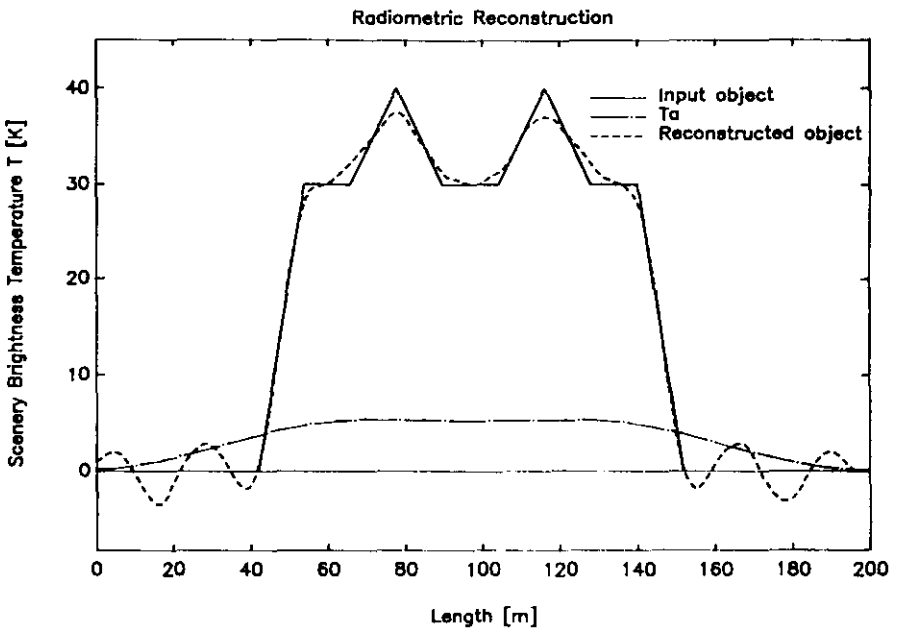

Figure 5.28. Ta determined with θ_a=1, θ_b=3. While the reconstruction is performed with θ_a=1 and θ_b=1.1×3.

As can be seen from these figures the reconstruction is rather insensitive for a small mismatch with respect to the shape of the main beam.

5.4 Comparing the results obtained with a focused and defocused antenna system

In the previous sections the reconstruction technique was tested with several input objects. Furthermore, the performance of the technique was demonstrated using a focused and a defocused antenna pattern. As mentioned before the reason for including a defocused antenna pattern was the possibility that shaping of the main lobe could affect the trade–off between resolution and accuracy of reconstruction. To be able to make a quantitative comparison the square error is calculated as follows:

$$\epsilon_{sq} = \frac{\sum_{i=1}^{N} [T(x_i) - T'(x_i)]^2}{\sum_{i=1}^{N} [T(x_i)]^2} \qquad x_i = i\frac{\text{length of T [m]}}{N} \tag{5.2}$$

Where T is the input signal (in this case the input signal is equal to the one used in figure 5.20), and T' the reconstructed signal. This error can be treated as a sort of signal to noise ratio ($(S/N)^{-1}$).

This error is calculated for the pattern given by Eq.(5.1) and for different defocused patterns as a function of resolution. The result is presented in Figure 5.29.
As can be seen in this figure results obtained with a defocused antenna system have larger errors than compared to those obtained with a focused antenna system.
So, defocussing of the antenna system does not appear to offer any advantages.

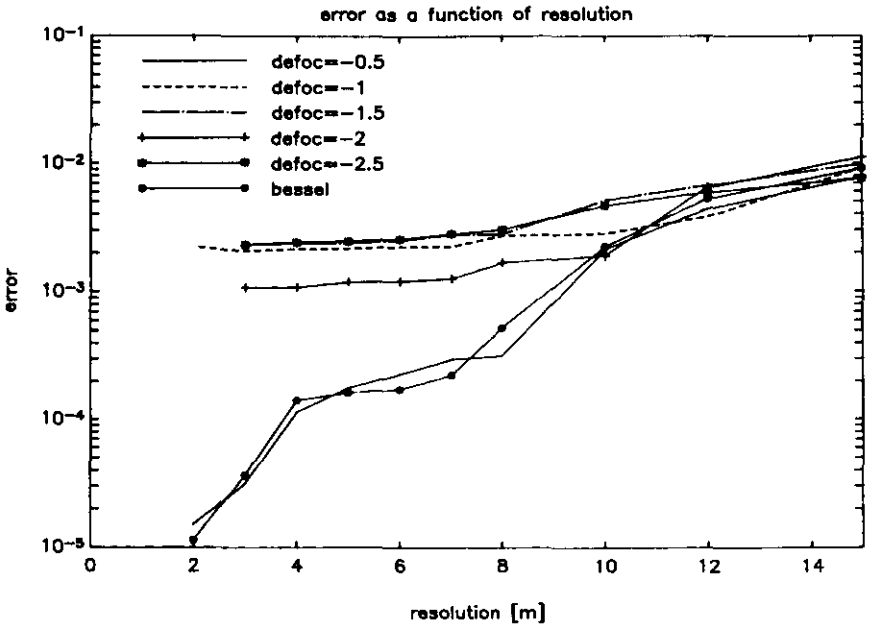

Fig 5.29. Square error as a function of resolution for different antenna patterns (focused and defocused).

6 Conclusions

A microwave radiometer inversion method has been presented. The method has been applied to various (noisy) input signals and results have been presented which show the capability of this methods in restoring spatial resolution. The effect of statistical errors in the antenna pattern on the results is reduced by spatial and time integration (averaging). The errors in the results due to systematic errors in G are shown to be of the same order of magnitude. The method presented here appears to have a nearly rectangular spatial transfer function. Special attention is given to the possible influence of shaping the main beam to the trade–off between resolution and accuracy of reconstrcution. Defocusing of the antenna system does not appear to offer any advantages in this trade–off.

References

[1] Stogryn, A.
ESTIMATES OF BRIGHTNESS TEMPERATURES FROM SCANNING RADIOMETER DATA.
IEEE Trans. Antennas Propag., vol.AP–26 (1978), p.720–726.

[2] Dittel, R.H.
DECONVOLUTION OF MICROWAVE RADIOMETRY DATA.
In: INVERSE METHODS IN ELECTROMAGNETIC IMAGING. Ed. by W.M. Boerner et al., Part 1. Dordrecht: D. Riedel, 1985. P.473–492.

[3] Nordius, H.
PHYSICAL INVERSION BY MEANS OF SINGULAR VALUE DECOMPOSITION OF A GROUND–BASED TEMPERATURE PROFILING MICROWAVE RADIOMETER.
In: MICROWAVE RADIOMETRY AND REMOTE SENSING APPLICATIONS.
Ed. by P. Pamploni. Utrecht: VSP, 1989. P.195–206.

[4] Bardati, F. and M. Mongiardo, D. Solimini.
ANTENNA PATTERN CORRECTION IN SCANNING RADIOMETRY: A singular system analysis.
Proc. IGARSS, Zürich, September 1986. P.595–598.

[5] Holmes, J.J. and C.A. Balanis, W.M. Truman.
APPLICATION OF FOURIER TRANSFORMS FOR MICROWAVE RADIOMETRIC INVERSIONS.
IEEE Trans. Antennas Propag., vol.AP–23 (1975), p.797–806.

[6] Zuhair Nashed, M.
OPERATOR–THEORETIC AND CIMPUTATIONAL APPROACHES TO ILL–POSED PROBLEMS WITH APPLICATIONS TO ANTENNA THEORY.
IEEE Trans. Antennas Propag., vol.AP–29 (1975), p.220–231.

[7] Orlanski, I.
A RATIONAL SUBDIVISION OF SCALE FOR ATMOSPHERIC PROCESSES.
Bull.Am.Meteorol.Soc., vol.56 (1975), p.527–530.

[8] Kuo, H.C.
DYNAMIC MODELING OF MARINE BOUNDARY LAYER CONVECTION.
Colorado State University, 1987 , Ph.D. thesis.

[9] Cotton, R.C. and R.A. Anthes.
STORM AND CLOUD DYNAMICS.
International Geophysics series, vol.44.
San Diego: Academic Press, 1989.

[10] Kitchen, M. and S.J. Caughey.
TEHTERED–BALLOON OBSERVATIONS OF THE STRUCTURE OF SMALL CUMULUS CLOUDS.
Q.J.R. Meteorol.Soc.,vol.107 (1981),p.853–874.

[11] Park, S.U. and D.N. Sikdar, V.E. Suomi.
CORRELATION BETWEEN CLOUD THICKNESS AND BRIGHTNESS USING NIMBUS–4 THIR DATA (11.4–μm CHANNEL) AND ATS 3 DIGITAL DATA.
Journal of Applied Meteorology, vol.13 (1974), p.402–410.

Appendix A : Writing the solution as a combination of shifted antenna patterns

A.1. The noise free problem

In Chapter 2 it was stated that the solution to the problem

$$G_i' \cdot T' = a_i \qquad i=(1,2,...N) \text{ and } \min||T'|| \tag{A.1}$$

resulted in a T'(x) which could be written as a linear combination of $G_i'(x)$. A geometrical motivation, will be given in this appendix.

All the functions T' that satisfy Eq.(1) form a function space V given by:

$$V = \{T' |\ G_i' \cdot T' = a_i\} \tag{A.2}$$

let V' be the linear manifold (a shifted version of V such that it contains the origin):

$$V' = \{v |\ G_i' \cdot v = 0\} \tag{A.3}$$

Then the space W perpendicular to V' is just the span of G_i' , i.e.

$$W = \{w |\ w \cdot v = 0,\ \forall\, v \in V'\} = \langle G_i' |\ i=1,..N\rangle \tag{A.4}$$

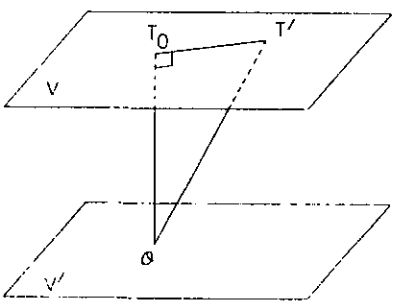

Figure A.1 The function spaces V and V'.

Then it follows from fig.A.1. that for all T' in V:

$$T_0 \perp (T'-T_0) \tag{A.5}$$

$$\text{Since } T'-T_0 \in V' \Rightarrow T_0 \in (V)^{\perp} = W \tag{A.6}.$$

So T_0 has to be an element of W and can be written as:

$$T_0 = \sum_{i=1}^{N} a_i G_i' \tag{A.7}$$

A.2 Including noise

If the problem is rearranged such that:

$$\left|\left| a_i - \frac{1}{4\pi}\int_{-\infty}^{\infty} T'(x)G_i'(x)\right|\right| = \epsilon \quad \text{and} \quad \min \int_{-\infty}^{\infty} T'^2(x)dx \tag{A.8}$$

The solution T is again a linear combination of the antenna patterns, this will be shown as follows:

PROOF

Suppose $\hat{T}$ is a solution (So $\hat{T}(x)$ is an ϵ good representation of $T'(x)$), and write:

$$\frac{1}{4\pi}\int_{-\infty}^{\infty} \hat{T}(x)G_i'(x) = \mu_i \tag{A.9}$$

Consider the following problem of finding a $T_0(x)$ which satisfies:

$$\frac{1}{4\pi}\int_{-\infty}^{\infty} T_0(x)G_i'(x) = \mu_i; \quad \min \int_{-\infty}^{\infty} T_0^2(x)dx \tag{A.10}$$

Referring to the prove given in section A.1, the solution to this problem is a unique linear combination of the antenna pattern:

$$T_0(x) = \sum_{i=1}^{N} a_i G_i'(x) \tag{A.11}$$

Now,

$$\left|\frac{1}{4\pi}\int_{-\infty}^{\infty} \hat{T}_0(x)G_i'(x) - a_i\right| = |\mu_i - a_i| = \left|\frac{1}{4\pi}\int_{-\infty}^{\infty} \hat{T}(x)G_i'(x) - a_i\right| \leq \epsilon_i \tag{A.12}$$

So $\hat{T}(x)$ also satisfies the conditions, so $T_0(x) = \hat{T}(x) = \sum_{i=1}^{N} a_i G_i'(x)$

Appendix B : The optimization problem including measurement errors

The problem is stated as:

$|| G\underline{a} - \underline{T}_a || \leq \epsilon$ and (B.1.a)

$\min 4\pi(\underline{a}^T G\underline{a})$ (B.1.b)

Suppose the vector $\underline{b}$ minimizes (B.1.b) and $|| G\underline{b} - \underline{T}_a || < \epsilon$

Let $\underline{a} = \gamma\underline{b}$ (B.2)

The left part of Eq.(B.1.a) can be written as:

$|| G\underline{a} - \underline{T}_a || = || \gamma G\underline{b} - \underline{T}_a || = || G\underline{b} - \underline{T}_a + (\gamma - 1)G\underline{b} ||$

Applying the triangle equality, leads to:

$||G\underline{b} - \underline{T}_a + (\gamma - 1)G\underline{b}|| \leq ||G\underline{b} - \underline{T}_a|| + ||(\gamma - 1)G\underline{b}||$ (B.3)

If $\gamma<1$ but close to 1 it is possible that Eq(B.3) still satisfies Eq.(B.1.a), the problem becomes:

$|| G\underline{b} - \underline{T}_a || + || (\gamma - 1)G\underline{b} || \leq \epsilon$

However

$\underline{a}^T G\underline{a} = \gamma^2 \underline{b}^T G\underline{b} < \underline{b}^T G\underline{b}$ (because $\lambda<1$)

which contradicts the fact that $\underline{b}$ was the minimum.

So if $\underline{b}$ satisfies Eq.(B.1.b) then it also satisfies

$|| G\underline{b} - \underline{T}_a || = \epsilon$

So the problem as stated in Eq.(B.1) is equivalent with the problem where the $\leq$ sign is replaced by the $=$ sign.

Appendix C: Influence of measurement errors in G

In this Appendix the influence of systematical errors originating from the finite measurement accuracy of the antenna pattern is discussed. As will be shown, the influence of these systematical errors is less prominent than the influence of statistical errors on the inversion method.

Again the problem is stated as:

$$|| G\underline{a} - \underline{T}_a || = \epsilon \qquad \text{and} \qquad \text{(C.1.a)}$$

$$\min || \underline{T}' || \implies \min 4\pi(\underline{a}^T G\underline{a}) \qquad \text{(C.1.b)}$$

With the help of the Lagrange multipliers it is possible to derive that the solution to this problem must satisfy:

$$|| G\underline{a} - \underline{T}_a || = \epsilon \qquad \text{and,} \qquad \text{(C.2.a)}$$

$$\underline{a} = \alpha(G\underline{a} - \underline{T}_a) \qquad \text{(C.2.b)}$$

Interesting to note is that if $||\underline{a}||$ is not small, α is proportional to $\frac{1}{||G\underline{a}-\underline{T}_a||} \propto \frac{1}{\epsilon}$. So, α is a large number.

The influence of errors in the matrix G (originating from the errors in the antenna pattern $G_i(x)$) on the inversion can be determined as follows:

$$\underline{a}+\delta\underline{a} = (\alpha+\delta\alpha)((G+\delta G)(\underline{a}+\delta\underline{a}) - \underline{T}_a) \qquad \text{(C.3)}$$

Neglecting higher order terms gives:

$$\delta\underline{a} = (I-\alpha G)^{-1}(G\underline{a}-\underline{T}_a)\delta\alpha + (I - \alpha G)^{-1}\alpha\, \delta G\underline{a} \qquad \text{(C.4)}$$

$$\delta\underline{a} = (I-\alpha G)^{-1}\frac{\delta\alpha}{\alpha}\,\underline{a} + (\frac{I}{\alpha} - G)^{-1}\delta G\,\underline{a} \qquad \text{(C.5)}$$

Where $(\frac{I}{\alpha} - G)^{-1}$ is nearly equal to G^{-1} because α is large and $(I-\alpha G)^{-1}$ gives no rise to problems because α is negative for the minimum.

$$\frac{||\delta\underline{a}||}{||\underline{a}\,||} \leq ||(I-\alpha G)^{-1}||\frac{\delta\alpha}{\alpha} + ||(\frac{I}{\alpha} - G)^{-1}||\;||\delta G|| \qquad \text{(C.6)}$$

$$\frac{||\delta\underline{a}||}{||\underline{a}\,||} \propto \mathcal{O}(||\delta G||) \qquad \text{(C.7)}$$

Consequently, this error can be made arbitrary small by putting effort in obtaining exact knowledge of the antenna pattern.

Appendix D : Errors due to incorrect estimation of the object velocity

Consider an error in v given by δv. Given Eq.(3.3) this will result in an δG which is proportional to :

$$\delta G_i'(x) \propto \left[\frac{1}{\tau} \int_{t-i\frac{\tau}{2}}^{t+i\frac{\tau}{2}} \int_{-\infty}^{\infty} \frac{\partial G(x+v_x\xi,y)}{\partial x} \, \xi \, dy d\xi \right] \delta v$$

where ∂ denotes the partial derivative. Because, the partial derivative of G is bounded, the following holds:

$$\delta G_i'(x) = \mathcal{O}\left(\left[\frac{1}{\tau} \int_{t-i\frac{\tau}{2}}^{t+i\frac{\tau}{2}} |\xi| d\xi \right] \delta v \right)$$

$$\Rightarrow$$

$$\delta G_i'(x) = \mathcal{O}(|t_i| \, \delta v)$$

Eq.(3.10) shows that this will lead to an error in the matrix G and in the previous appendix it was shown how to deal with those errors.

Appendix E: Flow diagrams of the algorithm

In this appendix flow diagrams of the reconstruction program are given. The notations used are nearly similar to the ones used in the report. In this appendix X(.) indicates the function X and X[.] indicates the array version of X. Furthermore, G(x,y) averaged over y is represented by G'(x) and G''(x) corresponds to the time averaged version of G'(x). The dimensions of all vectors are N and of all matrices N × N. In the flow diagrams x_{max} is used, which corresponds to the x–value of the outer circle of figure 2.3 (from figure 2.2 and 2.3 it is possible to derive that $R\tan(\theta)=\sqrt{x^2+y^2}$). LIL and UIL correspond to the lower integration limit ($-\sqrt{x_{max}^2-x^2}$) and upper integration limit($\sqrt{x_{max}^2-x^2}$), respectively. NF is the normalization factor to obtain a 4π normalized antenna pattern. Figure E.1 gives the flow diagram of the complete program and figures E.2 to E.7 give flow charts of parts of the program.

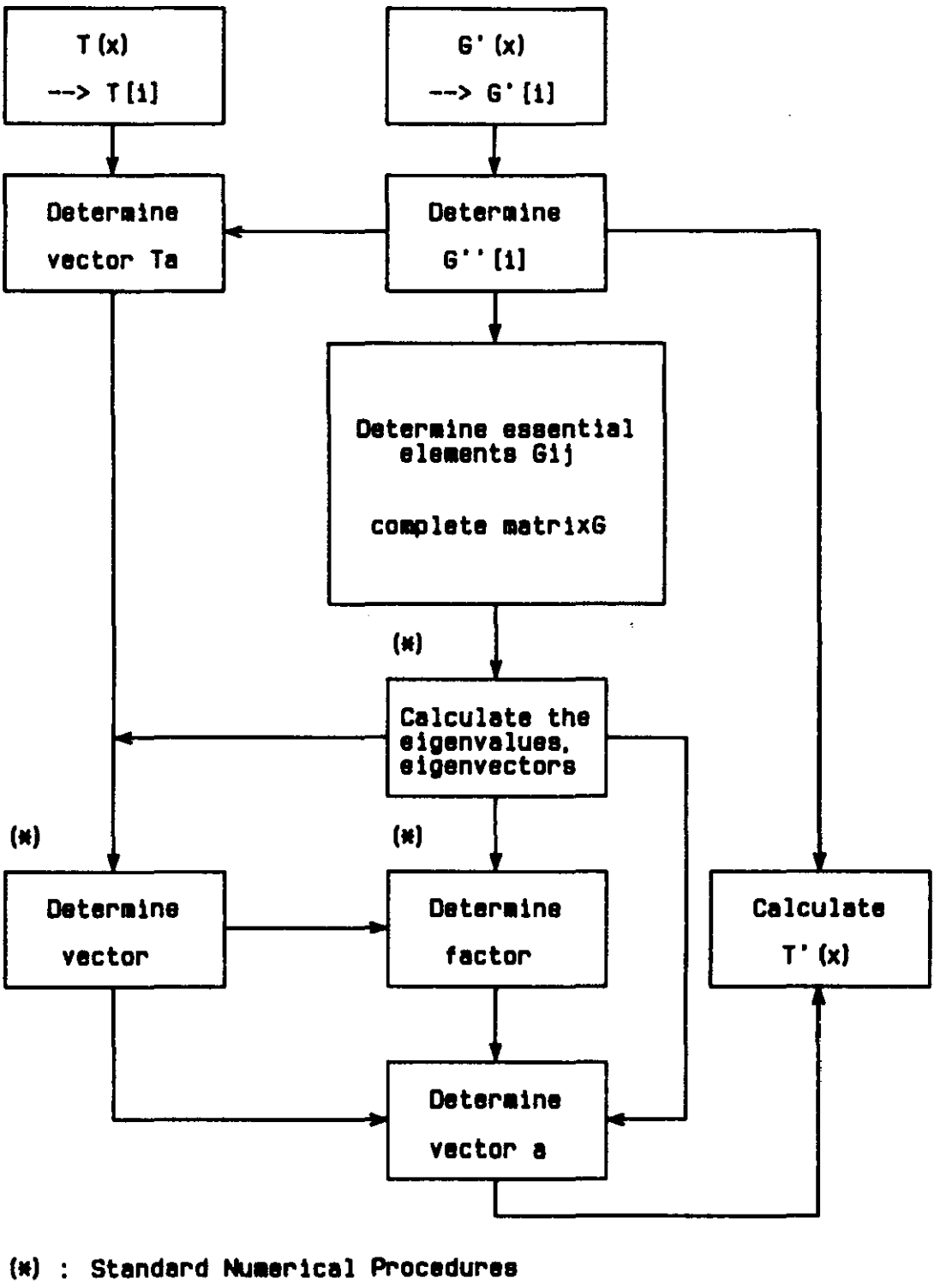

Fig. E.1. Flow digram of the complete reconstruction program.

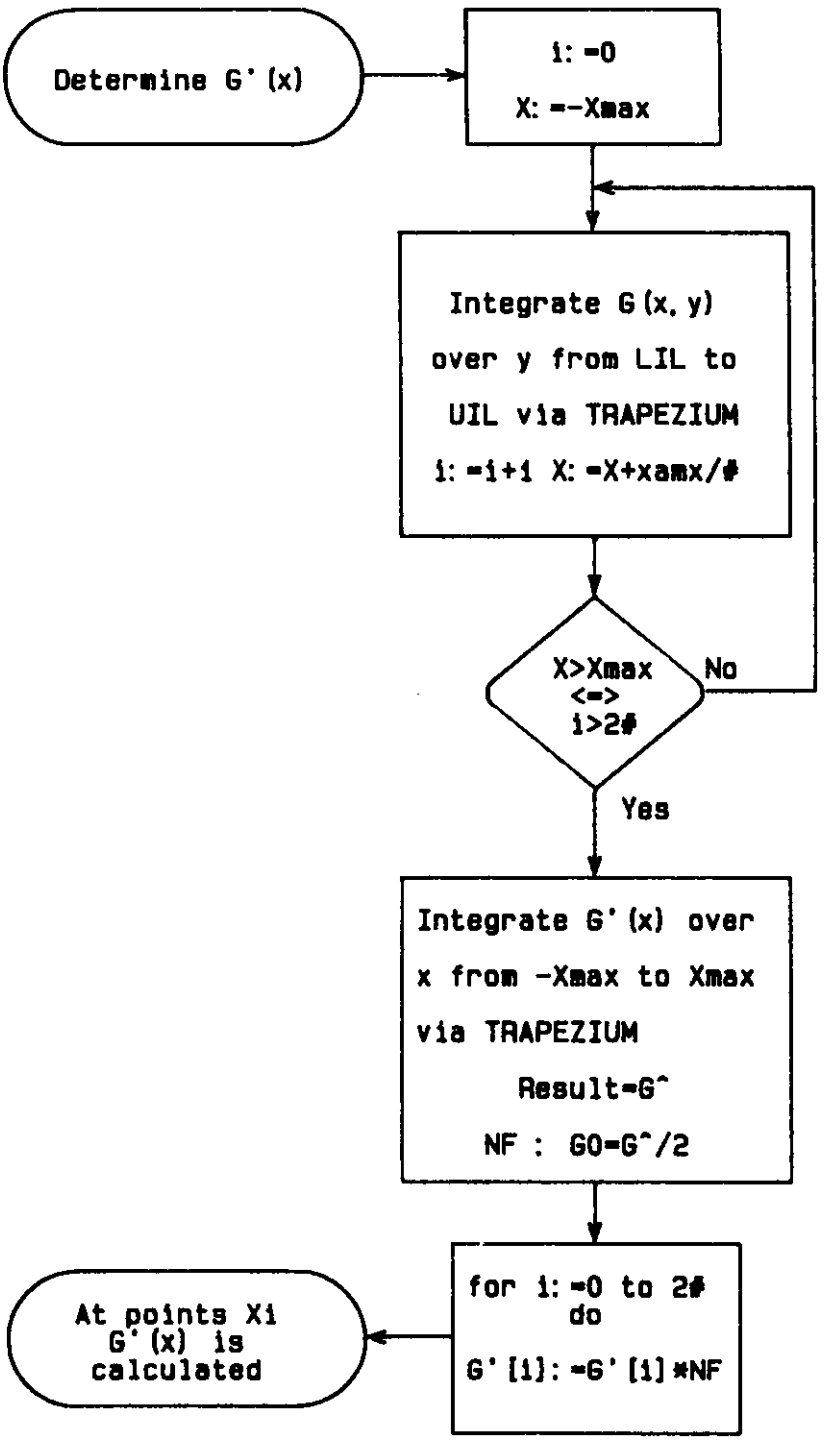

Fig. E.2. Flow digram of the determination of G(x) (= G(x,y) averaged over y).

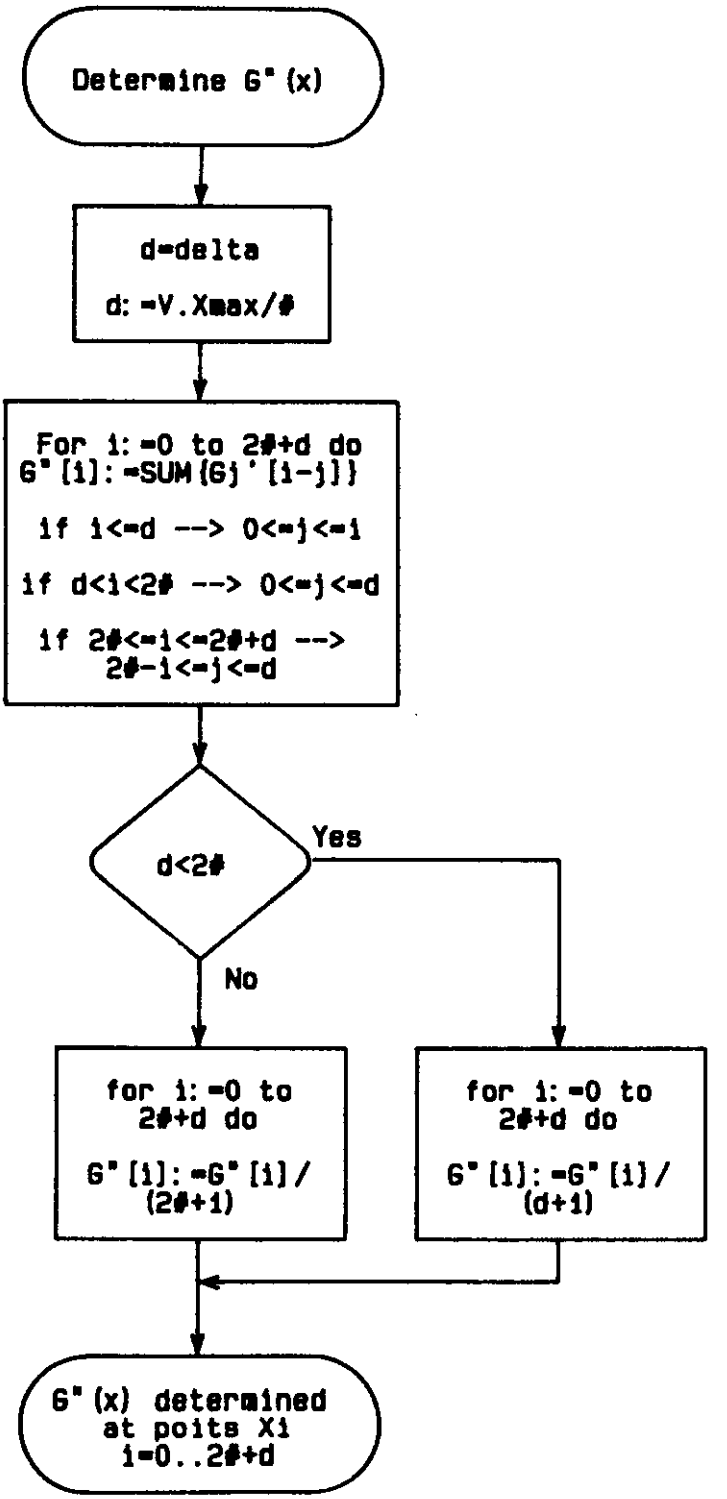

Fig. E.3. Flow digram of the determination of G'(x) (= G(x) averaged over time).

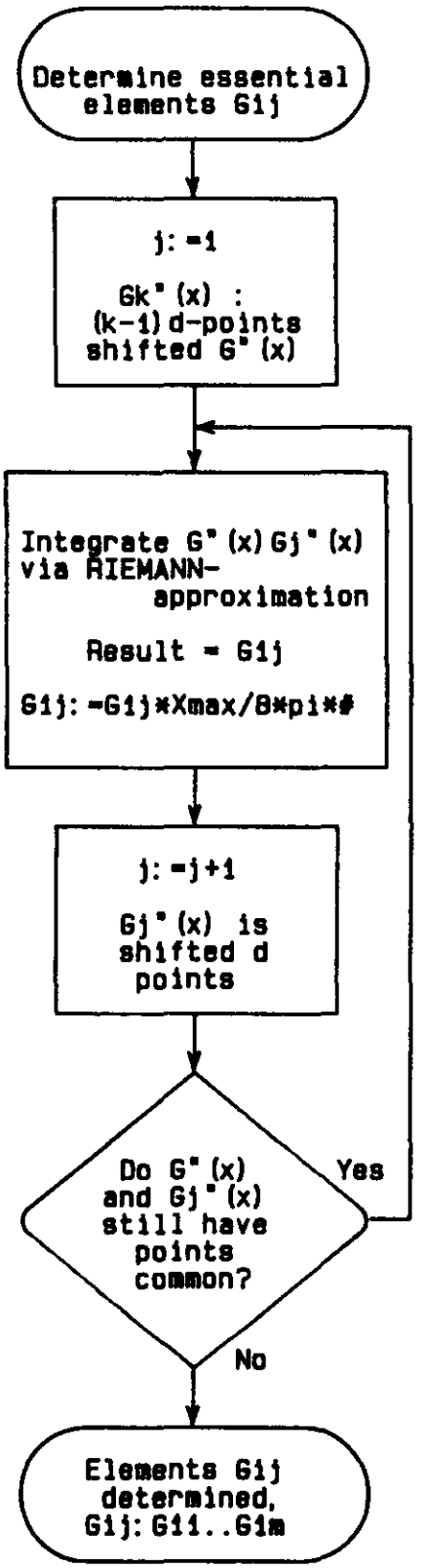

Fig. E.4. Flow digram of the determination of the matrix G.

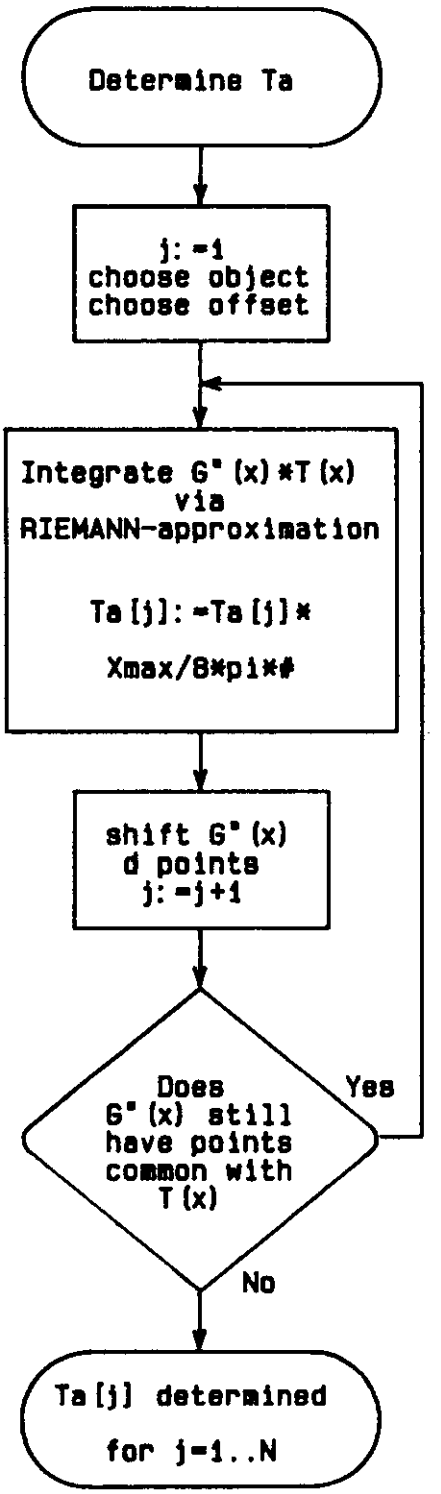

Fig. E.5. Flow digram of the determination of the signal T_a.

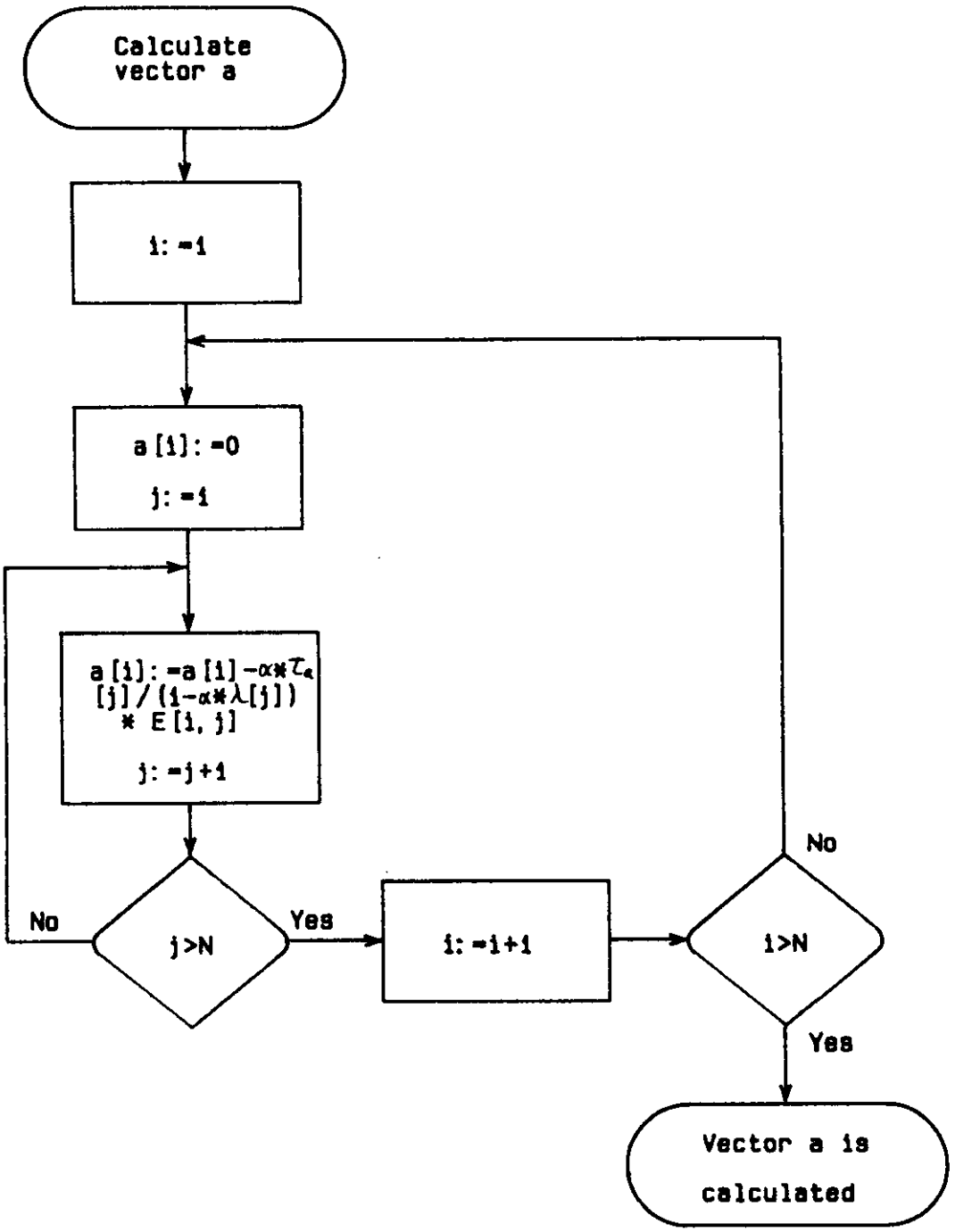

Fig. E.6. Flow digram of the determination of the vector a.

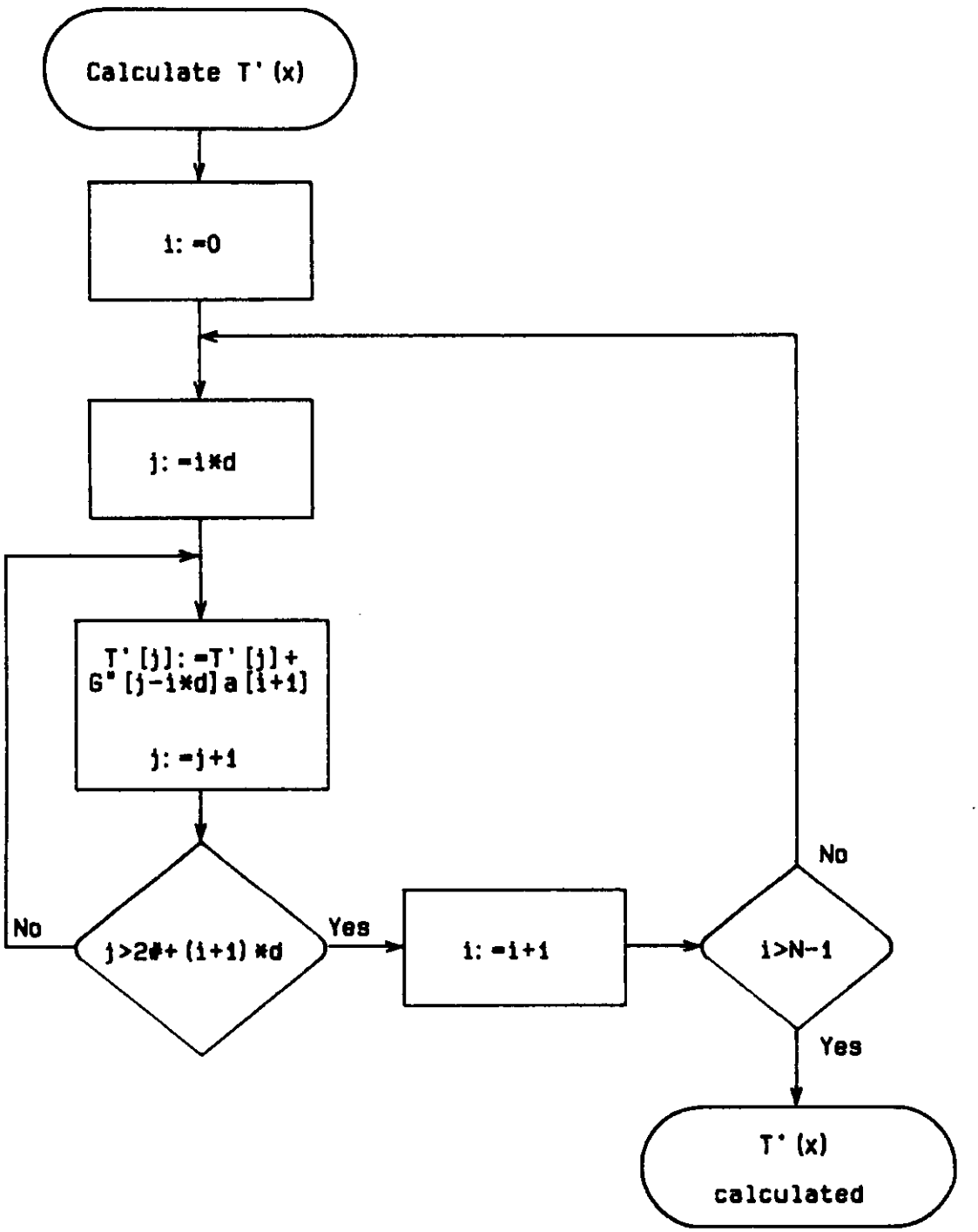

Fig. E.7. Flow digram of the determination of T'(x).

Eindhoven University of Technology Research Reports
Faculty of Electrical Engineering

ISSN 0167-9708
Coden: TEUEDE

(226) Dahiya, R.P. and E.M. van Veldhuizen, W.R. Rutgers, L.H.Th. Rietjens
EXPERIMENTS ON INITIAL BEHAVIOUR OF CORONA GENERATED WITH ELECTRICAL PULSES SUPERIMPOSED ON DC BIAS.
EUT Report 89-E-226. 1989. ISBN 90-6144-226-5

(227) Bastings, R.H.A.
TOWARD THE DEVELOPMENT OF AN INTELLIGENT ALARM SYSTEM IN ANESTHESIA.
EUT Report 89-E-227. 1989. ISBN 90-6144-227-3

(228) Hekker, J.J.
COMPUTER ANIMATED GRAPHICS AS A TEACHING TOOL FOR THE ANESTHESIA MACHINE SIMULATOR.
EUT Report 89-E-228. 1989. ISBN 90-6144-228-1

(229) Oostrom, J.H.M. van
INTELLIGENT ALARMS IN ANESTHESIA: An implementation.
EUT Report 89-E-229. 1989. ISBN 90-6144-229-X

(230) Winter, M.R.M.
DESIGN OF A UNIVERSAL PROTOCOL SUBSYSTEM ARCHITECTURE: Specification of functions and services.
EUT Report 89-E-230. 1989. ISBN 90-6144-230-3

(231) Schemmann, M.F.C. and H.C. Heyker, J.J.M. Kwaspen, Th.G. van de Roer
MOUNTING AND DC TO 18 GHz CHARACTERISATION OF DOUBLE BARRIER RESONANT TUNNELING DEVICES.
EUT Report 89-E-231. 1989. ISBN 90-6144-231-1

(232) Sarma, A.D. and M.H.A.J. Herben
DATA ACQUISITION AND SIGNAL PROCESSING/ANALYSIS OF SCINTILLATION EVENTS FOR THE OLYMPUS PROPAGATION EXPERIMENT.
EUT Report 89-E-232. 1989. ISBN 90-6144-232-X

(233) Nederstigt, J.A.
DESIGN AND IMPLEMENTATION OF A SECOND PROTOTYPE OF THE INTELLIGENT ALARM SYSTEM IN ANESTHESIA.
EUT Report 90-E-233. 1990. ISBN 90-6144-233-8

(234) Philippens, E.H.J.
DESIGNING DEBUGGING TOOLS FOR SIMPLEXYS EXPERT SYSTEMS.
EUT Report 90-E-234. 1990. ISBN 90-6144-234-6

(235) Heffels, J.J.M.
A PATIENT SIMULATOR FOR ANESTHESIA TRAINING: A mechanical lung model and a physiological software model.
EUT Report 90-E-235. 1990. ISBN 90-6144-235-4

(236) Lammers, J.O.
KNOWLEDGE BASED ADAPTIVE BLOOD PRESSURE CONTROL: A Simplexys expert system application.
EUT Report 90-E-236. 1990. ISBN 90-6144-236-2

(237) Ren Qingchang
PREDICTION ERROR METHOD FOR IDENTIFICATION OF A HEAT EXCHANGER.
EUT Report 90-E-237. 1990. ISBN 90-6144-237-0

(238) Lammers, J.O.
THE USE OF PETRI NET THEORY FOR SIMPLEXYS EXPERT SYSTEMS PROTOCOL CHECKING.
EUT Report 90-E-238. 1990. ISBN 90-6144-238-9

(239) Wang, X.
PRELIMINARY INVESTIGATIONS ON TACTILE PERCEPTION OF GRAPHICAL PATTERNS.
EUT Report 90-E-239. 1990. ISBN 90-6144-239-7

(240) Lutgens, J.M.A.
KNOWLEDGE BASE CORRECTNESS CHECKING FOR SIMPLEXYS EXPERT SYSTEMS.
EUT Report 90-E-240. 1990. ISBN 90-6144-240-0

(241) Brinker, A.C. den
A MEMBRANE MODEL FOR SPATIOTEMPORAL COUPLING.
EUT Report 90-E-241. 1990. ISBN 90-6144-241-9

(242) Kwaspen, J.J.M. and H.C. Heyker, J.I.M. Demarteau, Th.G. van de Roer
MICROWAVE NOISE MEASUREMENTS ON DOUBLE BARRIER RESONANT TUNNELING DIODES.
EUT Report 90-E-242. 1990. ISBN 90-6144-242-7

Eindhoven University of Technology Research Reports
Faculty of Electrical Engineering

ISSN 0167-9708
Coden: TEUEDE

(243) Massee, P. and H.A.L.M. de Graaf, W.J.M. Balemans, H.G. Knoopers, H.H.J. ten Kate
PREDESIGN OF AN EXPERIMENTAL (5-10 MWt) DISK MHD FACILITY AND PROSPECTS OF COMMERCIAL (1000 MWt) MHD/STEAM SYSTEMS.
EUT Report 90-E-243. 1990. ISBN 90-6144-243-5

(244) Klompstra, Martin and Ton van den Boom, Ad Damen
A COMPARISON OF CLASSICAL AND MODERN CONTROLLER DESIGN: A case study.
EUT Report 90-E-244. 1990. ISBN 90-6144-244-3

(245) Berg, P.H.G. van de
ON THE ACCURACY OF RADIOWAVE PROPAGATION MEASUREMENTS: Olympus propagation experiment.
EUT Report 90-E-245. 1990. ISBN 90-6144-245-1

(246) Maagt, P.J.I. de
A SYNTHESIS METHOD FOR COMBINED OPTIMIZATION OF MULTIPLE ANTENNA PARAMETERS AND ANTENNA PATTERN STRUCTURE.
EUT Report 90-E-246. 1990. ISBN 90-6144-246-X

(247) Józwiak, L. and T. Spassova-Kwaaitaal
DECOMPOSITIONAL STATE ASSIGNMENT WITH REUSE OF STANDARD DESIGNS: Using counters as sub-machines and using the method of maximal adjacensies to select the state chains and the state codes.
EUT Report 90-E-247. 1990. ISBN 90-6144-247-8

(248) Hoeijmakers, M.J. and J.M. Vleeshouwers
DERIVATION AND VERIFICATION OF A MODEL OF THE SYNCHRONOUS MACHINE WITH RECTIFIER WITH TWO DAMPER WINDINGS ON THE DIRECT AXIS.
EUT Report 90-E-248. 1990. ISBN 90-6144-248-6

(249) Zhu, Y.C. and A.C.P.M. Backx, P. Eykhoff
MULTIVARIABLE PROCESS IDENTIFICATION FOR ROBUST CONTROL.
EUT Report 91-E-249. 1991. ISBN 90-6144-249-4

(250) Pfaffenhöfer, F.M. and P.J.M. Cluitmans, H.M. Kuipers
EMDABS: Design and formal specification of a datamodel for a clinical research database system.
EUT Report 91-E-250. 1991. ISBN 90-6144-250-8

(251) Eijndhoven, J.T.J. van and G.G. de Jong, L. Stok
THE ASCIS DATA FLOW GRAPH: Semantics and textual format.
EUT Report 91-E-251. 1991. ISBN 90-6144-251-6

(252) Chen, J. and P.J.I. de Maagt, M.H.A.J. Herben
WIDE-ANGLE RADIATION PATTERN CALCULATION OF PARABOLOIDAL REFLECTOR ANTENNAS: A comparative study.
EUT Report 91-E-252. 1991. ISBN 90-6144-252-4

(253) Haan, S.W.H. de
A PWM CURRENT-SOURCE INVERTER FOR INTERCONNECTION BETWEEN A PHOTOVOLTAIC ARRAY AND THE UTILITY LINE.
EUT Report 91-E-253. 1991. ISBN 90-6144-253-2

(254) Velde, M. van de and P.J.M. Cluitmans
EEG ANALYSIS FOR MONITORING OF ANESTHETIC DEPTH.
EUT Report 91-E-254. 1991. ISBN 90-6144-254-0

(255) Smolders, A.B.
AN EFFICIENT METHOD FOR ANALYZING MICROSTRIP ANTENNAS WITH A DIELECTRIC COVER USING A SPECTRAL DOMAIN MOMENT METHOD.
EUT Report 91-E-255. 1991. ISBN 90-6144-255-9

(256) Backx, A.C.P.M. and Damen, A.A.H.
IDENTIFICATION FOR THE CONTROL OF MIMO INDUSTRIAL PROCESSES.
EUT Report 91-E-256. 1991. ISBN 90-6144-256-7

(257) Maagt, P.J.I. de and H.G. ter Morsche, J.L.M. van den Broek
A SPATIAL RECONSTRUCTION TECHNIQUE APPLICABLE TO MICROWAVE RADIOMETRY
EUT Report 92-E-257. 1992. ISBN 90-6144-257-5